Article

Hyperactivation of sympathetic nerves drives depletion of melanocyte stem cells

https://doi.org/10.1038/s41586-020-1935-3

Received: 22 May 2019

Accepted: 13 December 2019

Published online: 22 January 2020

Bing Zhang[1], Sai Ma[1,2,3], Inbal Rachmin[4], Megan He[1,5], Pankaj Baral[6], Sekyu Choi[1], William A. Gonçalves[7], Yulia Shwartz[1], Eva M. Fast[1,8], Yiqun Su[4], Leonard I. Zon[1,8,9], Aviv Regev[2,3,9], Jason D. Buenrostro[1], Thiago M. Cunha[6,10], Isaac M. Chiu[6], David E. Fisher[4] & Ya-Chieh Hsu[1]*

Empirical and anecdotal evidence has associated stress with accelerated hair greying (formation of unpigmented hairs)[1,2], but so far there has been little scientific validation of this link. Here we report that, in mice, acute stress leads to hair greying through the fast depletion of melanocyte stem cells. Using a combination of adrenalectomy, denervation, chemogenetics[3,4], cell ablation and knockout of the adrenergic receptor specifically in melanocyte stem cells, we find that the stress-induced loss of melanocyte stem cells is independent of immune attack or adrenal stress hormones. Instead, hair greying results from activation of the sympathetic nerves that innervate the melanocyte stem-cell niche. Under conditions of stress, the activation of these sympathetic nerves leads to burst release of the neurotransmitter noradrenaline (also known as norepinephrine). This causes quiescent melanocyte stem cells to proliferate rapidly, and is followed by their differentiation, migration and permanent depletion from the niche. Transient suppression of the proliferation of melanocyte stem cells prevents stress-induced hair greying. Our study demonstrates that neuronal activity that is induced by acute stress can drive a rapid and permanent loss of somatic stem cells, and illustrates an example in which the maintenance of somatic stem cells is directly influenced by the overall physiological state of the organism.

Stress has been anecdotally associated with a variety of changes in tissues, including hair greying. However, whether external stressors are the causal factors, and whether stress-related changes occur at the level of somatic stem cells, remain poorly understood. The hair follicle cycles between growth (anagen), degeneration (catagen) and rest (telogen)[5]. The bulge and hair germ region of the follicle contains two populations of stem cells: hair follicle stem cells (HFSCs), which are epithelial tissues, and melanocyte stem cells (MeSCs)[6], which are derived from the neural crest. HFSCs and MeSCs are normally quiescent except during early anagen, when they are activated concurrently to regenerate a pigmented hair[7,8]. Activation of HFSCs produces a new hair follicle. Activation of MeSCs generates differentiated melanocytes that migrate downwards, whereas MeSCs remain close to the bulge. At the hair bulb, differentiated melanocytes synthesize melanin to colour the newly regenerated hair from the root. At catagen, mature melanocytes are destroyed, leaving only the MeSCs that will initiate new rounds of melanogenesis in future cycles[9,10] (Extended Data Fig. 1a). The predictable behaviour of MeSCs and melanocytes, and the visible nature of hair colour, makes the melanocyte lineage an accessible model to investigate how stress influences tissue regeneration.

Diverse stressors induce hair greying

To examine whether psychological or physical stressors promote hair greying, we used three approaches to model stress in C57BL/6J mice with black coat colour: restraint stress[11,12], chronic unpredictable stress[13,14] and nociception-induced stress (which was achieved through an injection of resiniferatoxin (RTX), an analogue of capsaicin[15,16]). All three procedures led to increased numbers of unpigmented white hairs over time. Restraint stress and chronic unpredictable stress led to noticeable hair greying after three to five rounds of hair cycles. Nociception-induced stress produced the most pronounced and rapid effect—many new hairs that formed in the next hair cycle after RTX injection became unpigmented (Fig. 1a, b, Extended Data Fig. 1b, c).

Psychological or physical stressors trigger the adrenal glands to release stress hormones and catecholamines into the bloodstream[17]. In accordance with this, we detected an increase in both corticosterone (the primary glucocorticoid stress hormone in rodents that is equivalent to cortisol in humans) and noradrenaline (a catecholamine) in the blood of mice that were subjected to different stressors (Fig. 1c, Extended Data Fig. 1d), suggesting that our approaches induced classic stress responses.

[1]Department of Stem Cell and Regenerative Biology, Harvard University and Harvard Stem Cell Institute, Cambridge, MA, USA. [2]Klarman Cell Observatory, Broad Institute of MIT and Harvard, Cambridge, MA, USA. [3]Department of Biology and Koch Institute, Massachusetts Institute of Technology, Cambridge, MA, USA. [4]Cutaneous Biology Research Center, Department of Dermatology, Massachusetts General Hospital, Harvard Medical School, Charlestown, MA, USA. [5]Department of Molecular and Cellular Biology, Harvard University, Cambridge, MA, USA. [6]Department of Immunology, Harvard Medical School, Boston, MA, USA. [7]Institute of Biological Science, Federal University of Minas Gerais, Belo Horizonte, Brazil. [8]Stem Cell Program and Division of Hematology/Oncology, Boston Children's Hospital and Dana-Farber Cancer Institute, Harvard Medical School, Boston, MA, USA. [9]Howard Hughes Medical Institute, Chevy Chase, MD, USA. [10]Center for Research in Inflammatory Diseases (CRID), Department of Pharmacology, Ribeirão Preto Medical School, University of São Paulo, Ribeirão Preto, Brazil. *e-mail: yachieh_hsu@harvard.edu

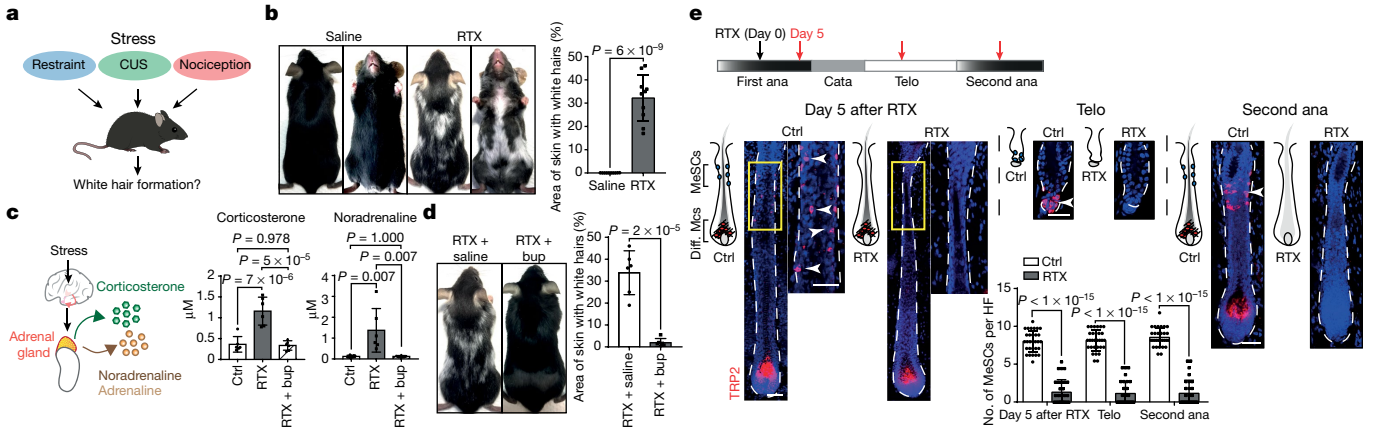

Fig. 1 | Stress depletes MeSCs. a, Black-coated C57BL/6J mice were subjected to different stress models. CUS, chronic unpredictable stress. **b**, Hair greying after injection of mice with RTX or saline. Right, quantification of the area of skin covered by white hairs ($n = 10$ mice for each condition, two-tailed unpaired *t*-test). **c**, Liquid chromatography with tandem mass spectrometry (LC–MS/MS) was used to quantify the concentration of serum stress hormones (corticosterone and noradrenaline) after injection of RTX alone or in combination with buprenorphine (bup) ($n = 6$ mice for each condition, one-way analysis of variance (ANOVA) with Tukey's multiple comparisons test). **d**, Injection of RTX with buprenorphine blocks formation of white hairs ($n = 6$ mice for each condition, two-tailed unpaired *t*-test). **e**, Top, experimental design (black arrow, RTX injection; red arrows, collection of skin samples). Bottom, immunofluorescent staining for TRP2 (a marker of the melanocyte lineage) in the hair follicle (HF) of control (ctrl, saline-injected) and RTX-injected mice ($n = 30$ hair follicles throughout the skin from 6 mice for each condition, two-way ANOVA with Benjamini–Hochberg correction). Yellow boxes denote the upper region of the hair follicle, where MeSCs reside. Enlarged views are shown to the right, and the number of MeSCs for each condition is quantified. Arrowheads denote MeSCs. Ana, anagen; cata, catagen; telo, telogen; diff. Mcs, differentiated melanocytes. Scale bars, 50 μm. All data are mean ± s.d.

RTX induces nociception by activating nociceptive sensory neurons[18]. Blocking the ability of mice to sense pain with buprenorphine (an opioid analgesic) prevented the increase of corticosterone and noradrenaline after RTX injection, suggesting that blocking pain sensation alleviates the physiological stress responses that are induced by RTX (Fig. 1c). Moreover, buprenorphine also suppressed the formation of white hairs in mice that were injected with RTX (Fig. 1d). These data show that regardless of the stress modality, premature hair greying can occur under stress. Because the effect of nociception induction on hair greying was the strongest and fastest of all the stressors we tested, we focused on RTX injection as our primary stressor.

Stress leads to loss of MeSCs

Loss of hair pigmentation can be due to defects in the synthesis of melanin[19,20], loss of differentiated melanocytes[21] or problems in the maintenance of MeSCs[22]. To understand how stress affects the melanocyte lineage, we injected RTX into mice during anagen, a stage in which both MeSCs and differentiated melanocytes were present but located within distinct compartments—MeSCs were near to the bulge, whereas differentiated melanocytes were at the hair bulb (Fig. 1e). After injection of RTX, $TRP2^+$ MeSCs were significantly reduced in number across the entire skin (Fig. 1e). In many hair follicles, MeSCs were completely lost from the bulge within five days, whereas differentiated melanocytes in the same hair follicle remained unperturbed (Fig. 1e, Extended Data Fig. 1e). These differentiated melanocytes continued to generate pigments, and the hair coat remained black five days after RTX injection (Extended Data Fig. 1f, g). When hair follicles in the RTX-injected mice entered catagen and telogen, many had lost all MeSCs (Fig. 1e). Subsequently, when the next round of anagen started, differentiated melanocytes were not produced to colour new hair shafts, and unpigmented hairs emerged (Fig. 1e, Extended Data Fig. 1h). Although some regenerated hairs remained pigmented, the numbers of MeSCs in these pigmented hairs were also reduced compared to those in mice not treated with RTX (Extended Data Fig. 1i). RTX injection led to the same extent of hair greying in both male and female mice (Extended Data Fig. 1j). Moreover, RTX also caused the loss of MeSCs when injected during telogen. In this case, unpigmented hairs appeared as soon as new hairs emerged in the following anagen (Extended Data Fig. 2a, b). These results suggest that MeSCs are exquisitely sensitive to RTX-induced stress, whereas differentiated melanocytes and the synthesis of melanin are not directly affected. MeSCs were also lost or reduced in mice that were subjected to restraint stress or chronic unpredictable stress (Extended Data Fig. 2c). Because stress depleted MeSCs, the loss of hair pigmentation in all three conditions was permanent (Extended Data Fig. 2d). Collectively, these data indicate that stress leads to loss of MeSCs.

Noradrenaline drives loss of MeSCs

Next, we asked how stress transmits to the periphery to alter MeSCs (Fig. 2a). Immune attack has been postulated to cause stress-induced hair greying[2,23]. To test the involvement of the immune system, we injected RTX into *Rag1* mutant mice, which lack both T and B cells, and into *CD11b-DTR* mice, in which myeloid lineages had been ablated by diphtheria toxin. Injection of RTX into these immune-deficient mice still resulted in formation of white hairs, suggesting that RTX-induced hair greying is independent of T cells, B cells or myeloid cells (Extended Data Fig. 3a, b).

As all stressors led to an increase in the levels of corticosterone and noradrenaline in the blood, we asked if these stress-induced circulating factors had a role in the stress-induced loss of MeSCs. RNA sequencing (RNA-seq) data from MeSCs that were purified by fluorescence-activated cell sorting (FACS) suggested that MeSCs express the glucocorticoid receptor (*GR*, also known as *Nr3c1*, a receptor for corticosterone) and the β_2-adrenergic receptor (*Adrb2*, a receptor for noradrenaline) (Extended Data Fig. 3c, Methods). To determine whether the glucocorticoid receptor mediated the effects of stress on MeSCs, we depleted this protein in MeSCs using Tyr–CreERT2—a tamoxifen-inducible CreERT2 fusion protein directed by a mouse tyrosinase promoter[8,24–26]. RTX injection into $Tyr^{creERT2}$;$GR^{fl/fl}$ mice still resulted in hair greying (Extended Data Fig. 3d). Moreover, no changes in MeSCs or hair pigmentation were observed when the levels of corticosterone were increased by feeding (Extended Data Fig. 3e). These data suggest that corticosterone is not a major driver of stress-induced loss of MeSCs.

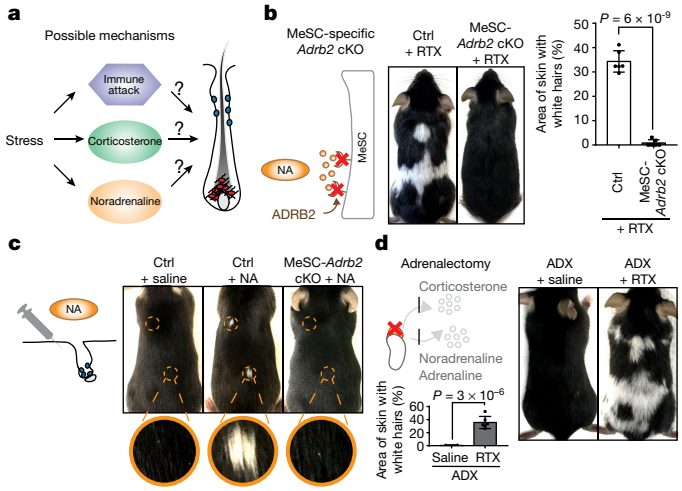

Fig. 2 | Noradrenaline drives hair greying. a, Possible mechanisms of loss of MeSCs. **b**, Injection of RTX into $Tyr^{creERT2}$;$Adrb2^{fl/fl}$ (MeSC-specific *Adrb2* conditional knockout (cKO)) mice does not trigger hair greying ($n = 6$ mice for each condition, two-tailed unpaired *t*-test). NA, noradrenaline. **c**, Formation of white hairs at sites of noradrenaline injection ($n = 10$ injected sites from 8 mice for each condition). For quantifications, see Extended Data Fig. 4e. Yellow dashed circles denote intradermal injection sites. **d**, Formation of white hairs after RTX injection in adrenalectomized mice (ADX) ($n = 6$ mice for each condition, two-tailed unpaired *t*-test). All data are mean ± s.d.

We then investigated whether ADRB2 might mediate the effect of stress on MeSCs. After injection of RTX, we observed a marked induction of phosphorylated CREB (a downstream effector of ADRB2) in MeSCs, but not in mature melanocytes (Extended Data Fig. 4a). Moreover, when we depleted ADRB2 from MeSCs using Tyr–CreERT2, white hairs did not form after RTX injection (Fig. 2b). These data suggest that ADRB2 expressed by MeSCs is essential for stress-induced hair greying. By contrast, when ADRB2 was depleted from hair follicle stem cells that share the same niche with MeSCs, RTX injection still resulted in hair greying (Extended Data Fig. 4b). In the absence of stress, depletion of ADRB2 in MeSCs did not lead to changes in MeSCs, melanocytes or pigment production, suggesting that the noradrenaline–ADRB2 pathway is dispensable for melanogenesis during the normal hair cycle (Extended Data Fig. 4c, d). Collectively, these data suggest that noradrenaline signals through ADRB2 on MeSCs to mediate stress-induced hair greying.

To test whether an increase in noradrenaline was sufficient to cause hair greying in the absence of stress, we introduced noradrenaline locally to the skin through intradermal injections. Local injection of noradrenaline promoted hair greying at the injection sites in wild-type mice and mice with HFSC-specific knockout of *Adrb2*, but did not cause hair greying in mice with MeSC-specific knockout of *Adrb2* (Fig. 2c, Extended Data Fig. 4e–g). Together, our data demonstrate that although immune cells and corticosterone are dispensable, noradrenaline signalling appears to be necessary for stress-induced hair greying and sufficient to trigger hair greying in the absence of stress.

Finding the source of noradrenaline

As the adrenal gland is a major source of noradrenaline under stress, to determine whether noradrenaline derived from the adrenal glands mediates stress-induced hair greying, we surgically removed both adrenal glands. Adrenalectomy significantly reduced the levels of corticosterone and noradrenaline in the bloodstream of RTX-injected mice (Extended Data Fig. 5a). However, injection of RTX into adrenalectomized mice still caused hair greying—suggesting that RTX-induced hair greying is independent of hormones or catecholamines from the adrenal glands (Fig. 2d).

An alternative source of noradrenaline is the sympathetic nervous system. Under stress, the sympathetic nervous system becomes activated to induce fight-or-flight responses through the secretion of noradrenaline from peripheral axon terminals[17]. In the skin, sympathetic nerves terminate close to the bulge where MeSCs reside (Fig. 3a). Furthermore, skin regions with high numbers of unpigmented hairs also have denser sympathetic innervation (Extended Data Fig. 5b).

To determine whether sympathetic nerves are indeed activated after RTX injection, we examined the levels of FOS, an immediate early transcription factor that serves as a reporter of neuronal activity[27]. Robust induction of FOS was detected in the cell bodies of sympathetic neurons within 1 hour of RTX injection, peaking at around 2–4 hours and diminishing after 24 hours, which suggests that RTX injection led to a burst activation of sympathetic neurons (Fig. 3b, Extended Data Fig. 5c). Moreover, when buprenorphine was injected together with RTX to block pain, FOS expression was not induced in sympathetic neurons (Fig. 3b). These data suggest that the sympathetic nervous system becomes highly activated following nociception-induced stress.

To test whether activation of sympathetic nerves is responsible for the loss of MeSCs and hair greying under stress, we used 6-hydroxy dopamine (6-OHDA)—a selective neurotoxin for sympathetic nerves[28]—to ablate sympathetic nerves. Sympathectomy blocked RTX-induced hair greying and loss of MeSCs (Fig. 3c, Extended Data Fig. 5d), suggesting that sympathetic nerves do mediate stress-induced hair greying. In addition, guanethidine—a chemical that blocks the release of noradrenaline from sympathetic nerve terminals[29]—suppressed hair greying and loss of MeSCs after RTX injection (Extended Data Fig. 5e). Collectively, these data suggest that noradrenaline secreted from sympathetic nerve terminals mediates the effect of stress on MeSCs.

To determine whether the activation of sympathetic nerves in the absence of stress is sufficient to drive the loss of MeSCs, we took a chemogenetic approach using the DREADDs (designer receptors exclusively activated by designer drugs) system[3,4]. G_q-DREADD is an artificial G_q-protein-coupled receptor that is activated by the inert molecule clozapine *N*-oxide (CNO), but not by endogenous ligands. Activation of G_q-DREADD leads to intracellular release of calcium and neuronal firing. We generated $TH^{creERT2}$;*CAG-LSL-*G_q*-DREADD*;$Rosa^{mT/mG}$ mice in which the sympathetic nerves can be activated artificially with CNO (Fig. 3d, Supplementary Discussion). Injection of CNO induced the activation of FOS in sympathetic ganglia, confirming the efficacy of this strategy (Extended Data Fig. 5f). Activation of sympathetic nerves with the DREADD system led to loss of MeSCs and hair greying at the sites where CNO was injected (Fig. 3d, Extended Data Fig. 5g). Moreover, when TH–CreERT2 was activated mosaically by a low dose of tamoxifen, intradermal CNO injection resulted in loss of MeSCs only in hair follicles innervated by DREADD-positive nerve fibres (recognizable by their expression of GFP in the membrane; Fig. 3e, Extended Data Fig. 5h). These data suggest that activation of sympathetic nerves in the absence of stressors is sufficient to drive the loss of MeSCs. Together, our findings suggest that increased noradrenaline secreted from the sympathetic nerve terminals drives the depletion of MeSCs under stress.

Stress drives hyperproliferation of MeSCs

Next, we aimed to identify the early changes in MeSCs under stress that might account for their loss (Fig. 4a). Immunofluorescence failed to detect active caspase-3 or TUNEL (terminal deoxynucleotidyl transferase dUTP nick end labelling) signals in MeSCs before their depletion from the niche after injection of RTX or noradrenaline. Moreover, RTX injection into *Ripk3* mutant mice, which lack a key kinase for necrosis, still caused hair greying (Extended Data Fig. 6a–c). These data suggest that stress-induced loss of MeSCs is not mediated by apoptosis or necrosis. Radiation causes DNA damage in MeSCs, and leads to their differentiation within the niche[22]. However, we failed to detect γ-H2AX

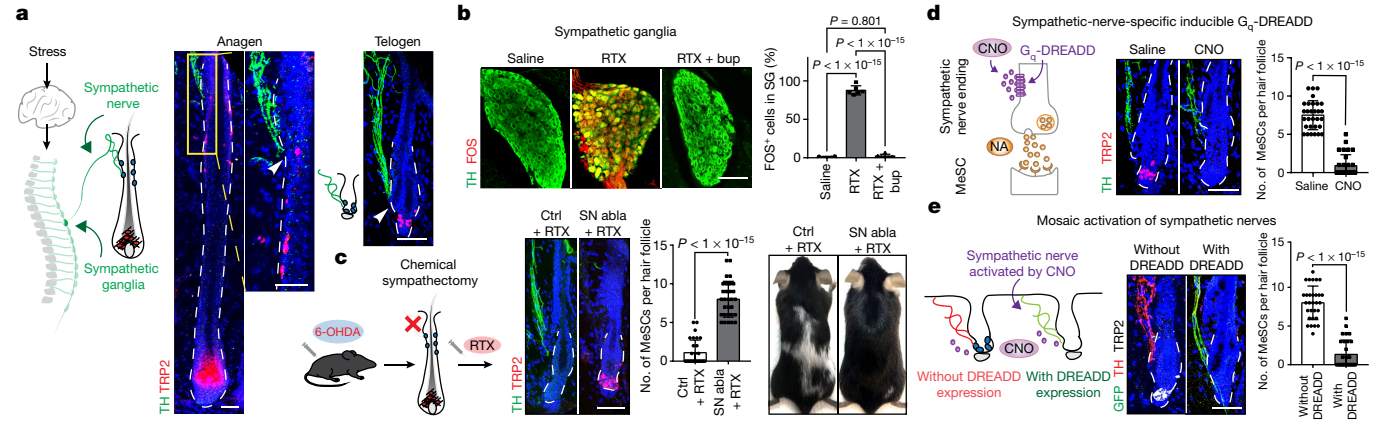

Fig. 3 | Hyperactivation of the sympathetic nervous system depletes MeSCs. **a**, Sympathetic nerves innervate MeSC niches. White arrowhead on the immunofluorescent staining indicates the close proximity of nerve endings to MeSCs ($n = 6$ mice for each condition). **b**, Left, immunofluorescent staining of sympathetic ganglia for tyrosine hydroxylase (TH; green) and FOS (red) from mice injected with saline, RTX and RTX with buprenorphine. Right, quantification of FOS$^+$ cells in sympathetic ganglia (SG) ($n = 6$ ganglia from 3 mice for each condition, one-way ANOVA with Tukey's multiple comparisons test). **c**, Injection of 6-hydroxydopamine (6-OHDA) blocks loss of MeSCs and induction of white hairs by RTX ($n = 30$ hair follicles from 6 mice for each condition, two-tailed unpaired *t*-test). SN abla, sympathetic nerve ablation. See also Extended Data Fig. 5d. **d**, Left, schematic of sympathetic nerve activation using a G_q-DREADD system. Right, immunofluorescent staining for TH (green) and TRP2 (red) from *TH^{creERT2};CAG-LSL-G$_q$-DREADD* mice treated with saline or CNO ($n = 30$ hair follicles from 6 mice for each condition, two-tailed unpaired *t*-test). **e**, Mosaic activation of sympathetic nerves in *TH^{creERT2};CAG-LSL-G$_q$-DREADD;Rosa$^{mT/mG}$* mice. Bar graphs quantify the number of MeSCs in hair follicles innervated by DREADD-negative sympathetic nerves (without DREADD) versus DREADD-positive sympathetic nerves (with DREADD; marked by membrane GFP expression) ($n = 30$ hair follicles for each condition from 4 mice, two-tailed unpaired *t*-test). Scale bars, 50 µm. All data are mean ± s.d.

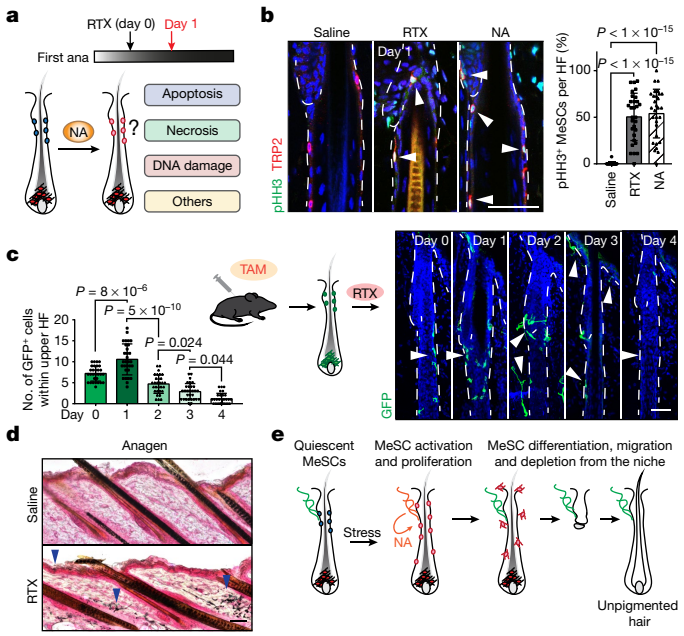

Fig. 4 | Noradrenaline drives MeSCs out of quiescence. **a**, Possible mechanisms by which noradrenaline depletes MeSCs. **b**, Left, immunofluorescent staining for phosphorylated histone H3 (pHH3, green) and TRP2 (red) one day after injection of RTX or noradrenaline. White arrowheads indicate the proliferative MeSCs. Right, quantification of pHH3$^+$ MeSCs ($n = 30$ hair follicles from 5 mice for each condition, one-way ANOVA with Tukey's multiple comparisons test). **c**, Time course of MeSC behaviour after treatment with RTX in *Tyr^{creERT2};Rosa$^{mT/mG}$* mice. White arrowheads mark MeSCs ($n = 30$ hair follicles from 3 mice for each time point, one-way ANOVA with Tukey's multiple comparisons test). TAM, tamoxifen. **d**, Fontana-Masson melanin staining five days after injection of saline or RTX ($n = 6$ mice for each condition). Blue arrowheads indicate ectopic pigments. **e**, Model summarizing steps of stress-induced MeSC depletion. Scale bars, 50 µm. All data are mean ± s.d.

foci (a hallmark of DNA damage) in MeSCs after injection of RTX or noradrenaline, which suggests that stress-induced depletion of MeSCs is not mediated through DNA damage (Extended Data Fig. 6d).

Quiescence is a key feature of many somatic stem cells[30–33], and loss of quiescence has been postulated to cause loss of MeSCs in *Bcl2* mutant mice[10,34]. To examine whether stress alters quiescence in MeSCs, we injected RTX or noradrenaline into mice that had entered full anagen (when MeSCs are normally quiescent). We saw a marked increase in the number of proliferating MeSCs within 24 hours of the injection of RTX or noradrenaline—about 50% of MeSCs became positive for phosphorylated histone H3, a marker of M phase (Fig. 4b). This number is in sharp contrast to the number of proliferating MeSCs in early anagen (about 6%), the only stage when MeSCs proliferate to self-renew[9,35] (Extended Data Fig. 6e). Conversely, no changes in proliferation or apoptosis were observed in mature melanocytes after injection of RTX or noradrenaline (Extended Data Fig. 6f, g). These data suggest that increased noradrenaline forces MeSCs to enter a rapid and abnormally proliferative state, but does not affect mature melanocytes.

To monitor changes in MeSCs after stress, we generated *Tyr^{creERT2};Rosa$^{mT/mG}$* mice, in which MeSCs can be traced by their membrane expression of GFP (Fig. 4c). Consistent with the observation that proliferation is an early response of MeSCs to stress, we saw a transient increase in GFP$^+$ cells shortly after RTX injection (Fig. 4c, day 1; quantified by FACS in Extended Data Fig. 6h). After this initial phase, many GFP$^+$ cells began to exhibit striking dendritic branching, which is a characteristic feature of differentiated MeSCs (Fig. 4c, day 2). They also began to move away from the bulge—some migrated downwards along the hair follicle, and some migrated out into the dermis or epidermis (Fig. 4c, days 2 and 3). By day 3, many GFP$^+$ cells had migrated out of the bulge, and by day 4, many hair follicles had lost all GFP$^+$ cells in the bulge. Moreover, ectopic pigmentation could be detected along the hair follicle, epidermis and dermis—areas that are normally devoid of pigments (Fig. 4d, Extended Data Fig. 6i). These data suggest that after stress, MeSCs undergo rapid proliferation followed by differentiation and migration, which leads to their loss from the niche (Fig. 4e, Supplementary Discussion).

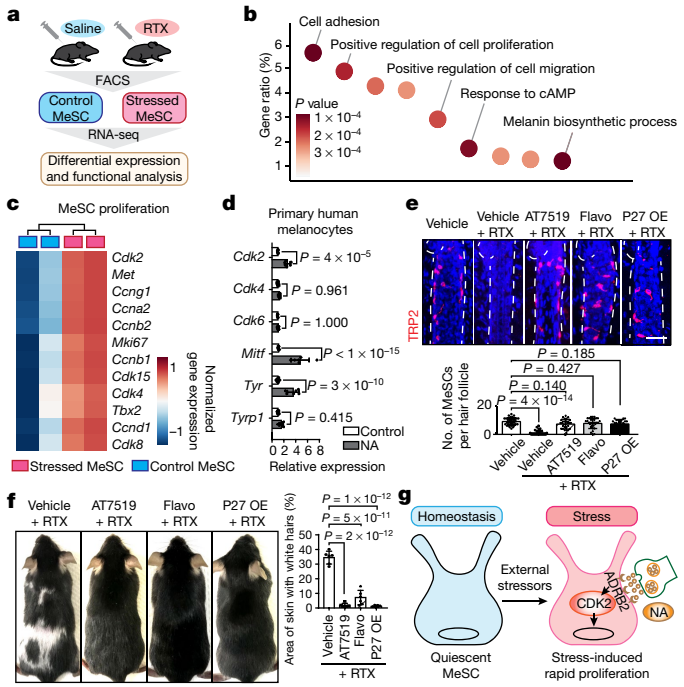

Fig. 5 | Inhibition of aberrant MeSC proliferation prevents stress-induced hair greying. a, Experimental workflow. FACS was performed in cells at telogen. **b**, GO enrichment analysis of significantly dysregulated genes in stressed MeSCs ($n = 2$ biologically independent samples for each condition, Fisher's exact test). **c**, Heat map of signature gene expression for genes that are related to the proliferation of MeSCs ($n = 2$ biologically independent samples for each condition). **d**, qRT–PCR of genes that are related to MeSC proliferation and differentiation in cultured primary human melanocytes treated with noradrenaline ($n = 6$ samples from 3 independent donors, two-way ANOVA with Benjamini–Hochberg correction). **e**, Top, immunofluorescent staining for TRP2 (red) from mice five days after treatment with RTX, RTX with CDK inhibitors (AT7519 or flavopiridol (flavo)) or RTX with MeSC-specific overexpression of P27 (P27 OE). Bottom, quantification of MeSCs ($n = 30$ hair follicles from 6 mice for each condition, one-way ANOVA with Tukey's multiple comparisons test). **f**, Topical treatment with AT7519, flavopiridol or MeSC-specific P27 overexpression inhibits RTX-induced hair greying ($n = 6$ mice for each condition, one-way ANOVA with Tukey's multiple comparisons test). **g**, Model summarizing the main findings of the study. Under strong external stressors, activated sympathetic nerves secrete noradrenaline that binds to ADRB2 on MeSCs. Noradrenaline–ADRB2 signalling drives rapid proliferation of MeSCs, followed by their ectopic differentiation and exhaustion. Scale bars, 50 μm. All data are mean ± s.d.

Transcriptome analyses of MeSCs

To discover the molecular mechanisms that drive stress-induced loss of MeSCs, we conducted RNA-seq using FACS-purified MeSCs from control and RTX-treated mice 12 hours after RTX injection, before MeSCs showed phenotypic differences (Fig. 5a, Extended Data Fig. 7a–c). Examination of the expression of marker genes for different types of skin cell confirmed that we had successfully enriched for MeSCs (Extended Data Fig. 7d). To uncover major molecular changes, we conducted Gene Ontology (GO) enrichment analysis (Fig. 5b). We also curated a list of known genes that are associated with the proliferation and differentiation of MeSCs (Fig. 5c, Extended Data Fig. 7e). Moreover, we used a list of genes that have previously been shown to be involved in entry into the cell cycle to assess whether regulators of the cell cycle are altered at the transcriptional level[36] (Extended Data Fig. 7f). Some of these key changes were also verified by quantitative PCR with reverse transcription (qRT–PCR) (Extended Data Fig. 7g). Collectively, we identified changes in several cell-cycle regulators in stressed MeSCs, including cyclin-dependent kinase 2 (*Cdk2*), which is a key promoter of the G1-to-S transition. Genes encoding receptors for ligands that promote the proliferation, differentiation and migration of MeSCs, including *Kit*[37] and *Mc1r*[38], were also upregulated. In addition, genes that are involved in melanogenesis[19], including *Mitf*, *Tyrp1*, *Tyr*, *Oca2* and *Pmel*, were upregulated (Fig. 5c, Extended Data Fig. 7e, g). These data suggest that MeSCs upregulate their proliferation and differentiation programs after stress. Furthermore, treatment with noradrenaline also led to a rapid induction of proliferation-associated genes such as *Cdk2* and differentiation-associated genes such as *Mitf* and *Tyr* in cultured human melanocyte cells (Fig. 5d). These data suggest that noradrenaline elicits similar responses in melanocyte lineages of both humans and mice.

Blocking proliferation preserves MeSCs

Because MeSCs first lose quiescence when under stress, we asked whether transient suppression of proliferation early in the stress response might prevent their depletion. We injected RTX at full anagen and applied CDK inhibitors (AT7519 or flavopiridol) topically to suppress proliferation transiently until 48 hours after injection[39,40]. MeSCs in RTX-injected mice that were treated with CDK inhibitors remained quiescent and were preserved in the niche (Fig. 5e, Extended Data Fig. 8a). Proliferation of cells in the hair bulb remained largely normal, probably because the penetration of inhibitors into subcutaneous regions in full anagen was limited (Extended Data Fig. 8b). To further confirm that loss of MeSCs can be prevented by inhibiting their proliferation, we generated a genetic mouse model, *Tyr*^{creERT2};*Rosa*$^{LSL\text{-}rtTA}$;*TetO*^{P27}, in which the CDK inhibitor P27 can be transiently induced with doxycycline in MeSCs. Induction of P27 expression in MeSCs suppressed their aberrant proliferation and preserved MeSCs in the niche under stress (Fig. 5e, Extended Data Fig. 8a). These preserved MeSCs showed an undifferentiated morphology and retained their functionality, as newly regenerated hairs in subsequent cycles maintained pigmentation (Fig. 5f). Together, these data suggest that loss of quiescence drives the depletion of MeSCs under conditions of stress, and that suppression of the proliferation of MeSCs is sufficient to prevent their loss.

Discussion

Acute stress is known to cause transient and beneficial fight-or-flight responses that are essential for survival. Here, we demonstrate that acute stress can also cause non-reversible depletion of somatic stem cells through activation of the sympathetic nervous system—resulting in permanent damage to tissue regeneration (Fig. 5g). Our findings support the emerging notion that the sympathetic nervous system not only regulates body physiology, but also influences a variety of processes in development and tissue maintenance[13,41–43]. The adrenal glands are the central regulators of stress responses. However, we show that the adrenal-gland-derived circulating stress hormones and catecholamines do not drive changes in MeSCs under stress. As sympathetic nerves innervate essentially all organs, acute stress might have a broad and rapid effect on many tissues through neuronal signals.

The reason for the existence of such an interaction between nerves and MeSCs is unknown. This said, the connection between the nervous system and pigment-producing cells is probably conserved during evolution. Cephalopods like squid, octopus and cuttlefish have sophisticated colouration systems that allow them to change colour for camouflage or communication. Neuronal activities control their pigment-producing cells (chromatophores), allowing rapid changes in colour in response to predators or threats[44]. Therefore, an attractive hypothesis is that sympathetic nerves might modulate MeSC activity, melanocyte migration or pigment production in situations independent of the hair cycle—for example, under bright sunlight or UV irradiation[45]. Under extreme stress, however, hyperactivation of neuronal activities overstimulates the pathway, which drives the depletion of MeSCs.

MeSCs also exhibit ectopic differentiation and depletion with age[10,20]. Of relevance, patients who have undergone partial sympathectomy develop fewer numbers of unpigmented hairs on the sympathectomized side with age[46,47]. In the future, it will be interesting to investigate whether the mechanisms that we have uncovered here also contribute to the loss of MeSCs that occurs during ageing, and whether stress might mimic an accelerated ageing process.

Online content

Any methods, additional references, Nature Research reporting summaries, source data, extended data, supplementary information, acknowledgements, peer review information; details of author contributions and competing interests; and statements of data and code availability are available at https://doi.org/10.1038/s41586-020-1935-3.

1. Ephraim, A. J. On sudden or rapid whitening of the hair. *AMA Arch. Derm.* **79**, 228–236 (1959).
2. Navarini, A. A., Nobbe, S. & Trüeb, R. M. Marie Antoinette syndrome. *Arch. Dermatol.* **145**, 656 (2009).
3. Alexander, G. M. et al. Remote control of neuronal activity in transgenic mice expressing evolved G protein-coupled receptors. *Neuron* **63**, 27–39 (2009).
4. Zhu, H. et al. Cre-dependent DREADD (designer receptors exclusively activated by designer drugs) mice. *Genesis* **54**, 439–446 (2016).
5. Müller-Röver, S. et al. A comprehensive guide for the accurate classification of murine hair follicles in distinct hair cycle stages. *J. Invest. Dermatol.* **117**, 3–15 (2001).
6. Hsu, Y.-C., Li, L. & Fuchs, E. Emerging interactions between skin stem cells and their niches. *Nat. Med.* **20**, 847–856 (2014).
7. Chang, C.-Y. et al. NFIB is a governor of epithelial-melanocyte stem cell behaviour in a shared niche. *Nature* **495**, 98–102 (2013).
8. Rabbani, P. et al. Coordinated activation of Wnt in epithelial and melanocyte stem cells initiates pigmented hair regeneration. *Cell* **145**, 941–955 (2011).
9. Nishimura, E. K. et al. Dominant role of the niche in melanocyte stem-cell fate determination. *Nature* **416**, 854–860 (2002).
10. Nishimura, E. K., Granter, S. R. & Fisher, D. E. Mechanisms of hair graying: incomplete melanocyte stem cell maintenance in the niche. *Science* **307**, 720–724 (2005).
11. Anthony, T. E. et al. Control of stress-induced persistent anxiety by an extra-amygdala septohypothalamic circuit. *Cell* **156**, 522–536 (2014).
12. Ramirez, S. et al. Activating positive memory engrams suppresses depression-like behaviour. *Nature* **522**, 335–339 (2015).
13. Heidt, T. et al. Chronic variable stress activates hematopoietic stem cells. *Nat. Med.* **20**, 754–758 (2014).
14. Tye, K. M. et al. Dopamine neurons modulate neural encoding and expression of depression-related behaviour. *Nature* **493**, 537–541 (2013).
15. Acs, G., Biro, T., Acs, P., Modarres, S. & Blumberg, P. M. Differential activation and desensitization of sensory neurons by resiniferatoxin. *J. Neurosci.* **17**, 5622–5628 (1997).
16. Baral, P. et al. Nociceptor sensory neurons suppress neutrophil and γδ T cell responses in bacterial lung infections and lethal pneumonia. *Nat. Med.* **24**, 417–426 (2018).
17. Ulrich-Lai, Y. M. & Herman, J. P. Neural regulation of endocrine and autonomic stress responses. *Nat. Rev. Neurosci.* **10**, 397–409 (2009).
18. Caterina, M. J. et al. The capsaicin receptor: a heat-activated ion channel in the pain pathway. *Nature* **389**, 816–824 (1997).
19. Kondo, T. & Hearing, V. J. Update on the regulation of mammalian melanocyte function and skin pigmentation. *Expert. Rev. Dermatol.* **6**, 97–108 (2011).
20. Steingrímsson, E., Copeland, N. G. & Jenkins, N. A. Melanocyte stem cell maintenance and hair graying. *Cell* **121**, 9–12 (2005).
21. Liao, C.-P., Booker, R. C., Morrison, S. J. & Le, L. Q. Identification of hair shaft progenitors that create a niche for hair pigmentation. *Genes Dev.* **31**, 744–756 (2017).
22. Inomata, K. et al. Genotoxic stress abrogates renewal of melanocyte stem cells by triggering their differentiation. *Cell* **137**, 1088–1099 (2009).
23. Harris, M. L. et al. A direct link between MITF, innate immunity, and hair graying. *PLoS Biol.* **16**, e2003648 (2018).
24. Bosenberg, M. et al. Characterization of melanocyte-specific inducible Cre recombinase transgenic mice. *Genesis* **44**, 262–267 (2006).
25. Köhler, C. et al. Mouse cutaneous melanoma induced by mutant BRaf arises from expansion and dedifferentiation of mature pigmented melanocytes. *Cell Stem Cell* **21**, 679–693 (2017).
26. Moon, H. et al. Melanocyte stem cell activation and translocation initiate cutaneous melanoma in response to UV exposure. *Cell Stem Cell* **21**, 665–678 (2017).
27. Sheng, M. & Greenberg, M. E. The regulation and function of c-*fos* and other immediate early genes in the nervous system. *Neuron* **4**, 477–485 (1990).
28. Kostrzewa, R. M. & Jacobowitz, D. M. Pharmacological actions of 6-hydroxydopamine. *Pharmacol. Rev.* **26**, 199–288 (1974).
29. Boullin, D. J., Costa, E. & Brodie, B. B. Discharge of tritium-labeled guanethidine by sympathetic nerve stimulation as evidence that guanethidine is a false transmitter. *Life Sci.* **5**, 803–808 (1966).
30. Acar, M. et al. Deep imaging of bone marrow shows non-dividing stem cells are mainly perisinusoidal. *Nature* **526**, 126–130 (2015).
31. Lay, K., Kume, T. & Fuchs, E. FOXC1 maintains the hair follicle stem cell niche and governs stem cell quiescence to preserve long-term tissue-regenerating potential. *Proc. Natl Acad. Sci. USA* **113**, E1506–E1515 (2016).
32. Wang, L., Siegenthaler, J. A., Dowell, R. D. & Yi, R. Foxc1 reinforces quiescence in self-renewing hair follicle stem cells. *Science* **351**, 613–617 (2016).
33. Cho, I. J. et al. Mechanisms, hallmarks, and implications of stem cell quiescence. *Stem Cell Reports* **12**, 1190–1200 (2019).
34. Nishimura, E. K. et al. Key roles for transforming growth factor β in melanocyte stem cell maintenance. *Cell Stem Cell* **6**, 130–140 (2010).
35. Takeo, M. et al. EdnrB governs regenerative response of melanocyte stem cells by crosstalk with Wnt signaling. *Cell Rep.* **15**, 1291–1302 (2016).
36. Tirosh, I. et al. Dissecting the multicellular ecosystem of metastatic melanoma by single-cell RNA-seq. *Science* **352**, 189–196 (2016).
37. Peters, E. M. J., Tobin, D. J., Botchkareva, N., Maurer, M. & Paus, R. Migration of melanoblasts into the developing murine hair follicle is accompanied by transient c-Kit expression. *J. Histochem. Cytochem.* **50**, 751–766 (2002).
38. Chou, W. C. et al. Direct migration of follicular melanocyte stem cells to the epidermis after wounding or UVB irradiation is dependent on Mc1r signaling. *Nat. Med.* **19**, 924–929 (2013).
39. Losiewicz, M. D., Carlson, B. A., Kaur, G., Sausville, E. A. & Worland, P. J. Potent inhibition of CDC2 kinase activity by the flavonoid L86-8275. *Biochem. Biophys. Res. Commun.* **201**, 589–595 (1994).
40. Wyatt, P. G. et al. Identification of *N*-(4-piperidinyl)-4-(2,6-dichlorobenzoylamino)-1*H*-pyrazole-3-carboxamide (AT7519), a novel cyclin dependent kinase inhibitor using fragment-based X-ray crystallography and structure based drug design. *J. Med. Chem.* **51**, 4986–4999 (2008).
41. Borden, P., Houtz, J., Leach, S. D. & Kuruvilla, R. Sympathetic innervation during development is necessary for pancreatic islet architecture and functional maturation. *Cell Rep.* **4**, 287–301 (2013).
42. Zeng, X. et al. Innervation of thermogenic adipose tissue via a calsyntenin 3β-S100b axis. *Nature* **569**, 229–235 (2019).
43. Katayama, Y. et al. Signals from the sympathetic nervous system regulate hematopoietic stem cell egress from bone marrow. *Cell* **124**, 407–421 (2006).
44. Reed, C. M. The ultrastructure and innervation of muscles controlling chromatophore expansion in the squid, *Loligo vulgaris*. *Cell Tissue Res.* **282**, 503–512 (1995).
45. Fan, S. M.-Y. et al. External light activates hair follicle stem cells through eyes via an ipRGC–SCN-sympathetic neural pathway. *Proc. Natl Acad. Sci. USA* **115**, E6880–E6889 (2018).
46. Lerner, A. B. Gray hair and sympathectomy. Report of a case. *Arch. Dermatol.* **93**, 235–236 (1966).
47. Ortonne, J. P., Thivolet, J. & Guillet, R. Graying of hair with age and sympathectomy. *Arch. Dermatol.* **118**, 876–877 (1982).

Methods

Randomization

The mice were randomly assigned into different experimental groups whenever possible, except in experiments that required specific genotypes (in this case, sex-matched littermate controls were used).

Blinding

For LC–MS/MS analysis, RNA-seq library preparation and sequencing, experimenters were blinded to experimental conditions. Blinding was not possible in mouse studies owing to the need to identify specific genotypes or treat mice with different chemicals according to experimental designs.

Mice

C57BL/6J, *Tyr*^{creERT2}, *K15*^{crePGR}, *Rag1* mutant, *CD11b-DTR*, *GR*$^{fl/fl}$, *CAG-LSL-G*$_q$*-DREADD*, *Rosa*$^{H2B\text{-}GFP/GPI\text{-}mCherry}$, *Rosa26*$^{mT/mG}$, *Rosa*$^{LSL\text{-}rtTA}$ and *Ripk3* mutant mice were obtained from the Jackson Laboratory. *Adrb2*$^{fl/fl}$ mice[48] were originally generated by G. Karsenty (Columbia University) and provided to us by P. Frenette (Albert Einstein College of Medicine). *TH*^{creERT2} mice[49] were generated and provided by D. Ginty (Harvard Medical School). *TetO*^{P27} mice[50] were originally generated by G. Cady (Roswell Park Cancer Institute) and provided to us by V. Greco (Yale School of Medicine). All experiments used balanced groups of male and female mice. All experiments were conducted using mice at the same stage of the hair cycle and in a comparable age range (postnatal day (P)20–P25 for first telogen, P31–P36 for full anagen and P50–P60 for second telogen, or long-term monitoring as specified). To monitor the hair cycle, mice were shaved at weaning to monitor changes in skin colour, and these were confirmed by skin sections. The acquisition of human melanocyte cells was carried out in accordance with the Institutional Review Board policies at Massachusetts General Hospital. All mice were maintained in an animal facility approved by the Association for Assessment and Accreditation of Laboratory Animal Care at Harvard University, Harvard Medical School and Ribeirao Preto Medical School. Procedures were approved by the Institutional Animal Care and Use Committee of all institutions and complied with all relevant ethical regulations.

Stress procedures

Restraint and chronic unpredictable stress procedures were performed as previously described[11–14]. In brief, for restraint stress, C57BL/6J mice were kept in a restrainer (Thermo Fisher Scientific 12972590) for four hours per day for five days starting from mid-anagen (P28–P30). Hairs were depilated to induce hair regeneration when their hair cycle reached telogen. Mice were stressed and depilated four rounds in total to monitor long-term changes. For chronic unpredictable stress, C57BL/6J mice were exposed to a combination of stressors. Two of the stressors were applied each day. The stressors included cage tilt, isolation, damp bedding, rapid light and dark changes, overnight illumination, restraint, empty cage and changing the cage three times. All stressors were randomly repeated in consecutive weeks.

Drug treatments

For RTX treatment (see also Supplementary Discussion), mice received injections of RTX (30–100 μg kg^{-1}) in the flank for 1–3 days, as described previously[15,16,51–56]. RTX was prepared in 2% DMSO with 0.15% Tween 80 in PBS. Control mice were treated with the vehicle only. RTX injection was done either in full anagen (P31–P36) or in first telogen (P21). For corticosterone feeding, 35 μg ml^{-1} corticosterone (Millipore Sigma, C2505) was dissolved in 0.45% hydroxypropyl-β-cyclodextrin and provided in the drinking water. Mice were treated for three days (P28–P30). Control mice received the vehicle water (0.45% β-cyclodextrin). For analgesia, mice were injected with buprenorphine (0.1 mg kg^{-1}) 4 h before RTX injection and every 6 h after RTX injection for 2 days. For tamoxifen treatment, tamoxifen was diluted in corn oil to a final concentration of 20 mg ml^{-1}. To induce recombination, 20 mg kg^{-1} was injected intraperitoneally once per day for 4–7 days. For mosaic induction of Tyr–CreERT2 and TH–CreERT2, 20 mg kg^{-1} tamoxifen was injected intraperitoneally once per day for 3 days. For intradermal noradrenaline injection, noradrenaline (Sigma-Aldrich 489350) solution was prepared freshly by dissolving in 0.1% ascorbic acid in 0.9% sterile NaCl to a final concentration of 2 mM. Fifty microlitres was injected intradermally into experimental mice together with fluorescent beads at full anagen (around P31–P36). Control mice were injected with an equivalent volume of vehicle (0.1% ascorbic acid in 0.9% sterile NaCl) with fluorescent beads. The injection sites were marked using water-resistant ink. For ablation of sympathetic nerves, 6-hydroxydopamine hydrobromide (6-OHDA, Sigma 162957) solution was prepared freshly by dissolving 6-OHDA in 0.1% ascorbic acid in 0.9% sterile NaCl. Mice were injected intraperitoneally with 6-OHDA (100 mg per kg body weight) daily from P18 to P22. Control mice were injected with an equivalent volume of vehicle (0.1% ascorbic acid in 0.9% sterile NaCl). Ablation efficiency in the skin was confirmed by immunofluorescence staining. For guanethidine treatment, mice were intraperitoneally injected with 30 mg per kg body weight of guanethidine (Sigma-Aldrich, 1301801), once a day for 3 consecutive days before RTX administration at full anagen (around P31–P36). For induction of G_q-DREADD, 50 μl CNO (1 mg ml^{-1} in 0.9% sterile saline) was injected intradermally into experimental mice, together with fluorescent beads at full anagen (around P31–P36). Control mice were injected with an equivalent volume of vehicle (0.9% sterile saline) together with fluorescent beads. For administration of diphtheria toxin, diphtheria toxin (Sigma-Aldrich) was dissolved in 0.9% saline (0.1 mg ml^{-1}). For ablation, *CD11b-DTR* transgenic mice were intraperitoneally injected with diphtheria toxin (25 ng per g body weight) daily 3 days before RTX injection at full anagen (around P31–P36). Diphtheria toxin (20 ng per g body weight) was injected every 3 days after RTX injection until collection of skin samples. For inhibitor treatment, mice were shaved and pre-treated with AT7519 (Cayman Chemical 16231) or flavopiridol (Cayman Chemical 10009197) (both 5 mg per kg body weight) in ethanol topically 48 h and 24 h before RTX injection, at the time of RTX injection and 24 h and 48 h after injection. For induction of P27 expression, mice were fed with the doxycycline rodent diet (VWR 89067-462) for three days before RTX treatment and three days after. RTX was given at Anagen VI (around P31–P36).

Quantification of unpigmented hairs

For restraint and chronic unpredictable stress, unpigmented hairs were quantified by plucking around 100 hairs from 3 or 4 regions of the skin across the anterior to posterior end, and the percentage of white hairs was calculated by dividing the number of white hairs by the total number of hairs plucked. For RTX injection experiments, the percentage of regions with white hairs was calculated by dividing the size of areas with white hairs by the size of the whole skin (both areas were measured using ImageJ). For intradermal injection experiments (noradrenaline or CNO), unpigmented hairs were quantified by plucking around 100 hairs from each injection site (marked by water-resistant ink at the time of injection), and the percentage of white hairs was calculated by dividing the number of white hairs by the total number of hairs plucked.

Histology and immunohistochemistry

Mouse skin samples were fixed using 4% paraformaldehyde (PFA) for 15 min at room temperature, washed 6 times with PBS and immersed in 30% sucrose overnight at 4 °C. Samples were then embedded in optimal cutting temperature (OCT) compound (Sakura Finetek). Sections of approximately 35–50 μm were fixed in 4% paraformaldehyde (PFA) for 2 min and washed with PBS and 0.1% Triton X-100 in PBS. Slides were then blocked using blocking buffer (5% donkey serum; 1% BSA, 2% cold water fish gelatin in 0.3% Triton X-100 in PBS) for 1 h at room temperature, followed by staining with primary antibodies overnight at 4 °C and secondary antibody for 4 h at room temperature. For quantification

of the density of sympathetic nerves, 90-μm sections were used. The TUNEL assay was performed according to the manufacturer's instructions (Roche). Fontana-Masson staining was performed according to the manufacturer's instructions (Market Lab ML7255). Antibodies used: TRP2 (Santa Cruz 10451, 1:800), tyrosine hydroxylase (rabbit, Millipore AB152, 1:1,000 or sheep, Millipore AB1542, 1:150–1:300), FOS (Abcam, 190289, 1:1,000), γ-H2AX (Cell Signaling, 9718, 1:400), phosphorylated histone H3 (rabbit, Cell Signaling Technology 3377S, 1:500), cleaved caspase 3 (rabbit, Cell Signaling Technology 9664S, 1:400), GFP (rabbit, Abcam ab290, 1:1,000 or chicken, Aves labs GFP-1010, 1:200), CD3 (eBioscience 14-0032-81, 1:800), CD11B (eBioscience 14-0112-81, 1:800), phosphorylated CREB (Cell Signaling 9198, 1:800) and MITF (Abcam ab12039, 1:400).

Measurement of stress hormones

A sample of 50 μl of blood plasma was collected from each mouse and transferred into a 1.5-ml microcentrifuge tube. Ten microlitres of internal solution was added to each sample followed by 100 μl water and 640 μl methanol. Samples were incubated at −20 °C for 1 h, then centrifuged for 30 min at maximum speed at −9 °C. The supernatant was transferred to a new tube and dried under N2 flow, then resuspended in 50 μl methanol and transferred to micro-inserts. All samples were run on an Agilent 6460 Triple Quad LC/MS with an Agilent 1290 Infinity HPLC. For corticosterone-treated mice, plasma corticosterone levels were determined by ELISA according to the manufacturer's instructions (Arbor Assays, K014-H1).

Radiation

Ten-week-old C57BL/6J mice were gamma-irradiated (^{137}Cs source) with a dose of 10.5 Gy. Mice were transplanted with 300,000 whole bone marrow cells to ensure survival after lethal irradiation.

FACS

Mouse dorsal skin was collected, and the fat layer was removed by gentle scraping from the dermal side. The skin was incubated in 0.25% collagenase in Hank's balanced salt solution (HBSS) at 37 °C for 35–45 min on an orbital shaker. Single-cell suspension was collected by gentle scraping of the dermal side and filtering through 70-μm and 40-μm filters. The epidermal layer was incubated in trypsin-EDTA at 37 °C for 35–45 min on an orbital shaker. Single-cell suspension was collected by gentle scraping of the epidermal side and filtering through 70-μm and 40-μm filters. The single-cell suspension was centrifuged for 5 min at 4 °C, resuspended in 0.25% FBS in PBS and stained with fluorescent-dye-conjugated antibodies for 30 min. For late anagen skin samples, the bottom parts of the hair follicles, containing mature melanocytes, were removed by gentle scraping under a dissection microscope. The MeSCs located close to the bulge remained and were verified by immunostaining. Antibodies used: CD140A (Invitrogen 13-1401-82, 1:200), CD45 (Invitrogen 13-0451-82, 1:400), SCA1 (Invitrogen 13-5981-82, 1:1,000), CD34 (Invitrogen 13-0341-82, 1:100), CD117 (Biolegend 135136, 1:400). See a published protocol for detailed instructions[57].

RNA isolation

RNA was isolated using a RNeasy Micro Kit (Qiagen) with QIAcube according to the manufacturer's instructions. RNA concentration and RNA integrity were determined by Bioanalyzer (Agilent) using the RNA 6000 Nano chip. High-quality RNA samples with an RNA integrity number of 8 or higher were used as input for RT–PCR and RNA-seq.

Cell culture

Primary human melanocytes were derived from neonatal foreskin as previously described[58] and cultured in Medium 254 (Invitrogen, Thermo Fisher Scientific). Melanocytes (passages 2 and 4) were starved for 24 h in Ham's F-10 nutrient mixture with 1% penicillin–streptomycin–glutamine before the addition of noradrenaline (10 μM).

qRT–PCR

The cDNA libraries were synthesized using Superscript IV VILO master mix with ezDNase (Thermo Fisher Scientific). qPCR was performed using power SYBR green (Thermo Fisher Scientific) on an ABI QuantStudio6 Flex qPCR instrument. C_t values were normalized to an internal control of β-actin (Actb).

Imaging and image analysis

All images were acquired using a Zeiss LSM 880 confocal microscope or Keyence microscope with ×20 or ×40 magnification lenses. Images are presented as maximum intensity projection images. For colocalization analysis, images are presented as a single *z*-stack. For quantification of the density of sympathetic nerves, tyrosine hydroxylase staining of sympathetic nerves was performed on samples of skin sections (90-μm thickness) to ensure the capture of all fibres innervating each hair follicle. Sympathetic nerves innervating individual hair follicles were selected and imaged using a Zeiss LSM 880 confocal microscope. Three-dimensional (3D) surfaces of tyrosine hydroxylase staining were created using Imaris x64 9.3.0 software and the volume was measured and compared. To quantify cell numbers (MeSC numbers, cell death events, proliferation events) within a hair follicle, immunofluorescence staining images of skin sections from multiple regions across the body were used. The number of cells was counted manually or by using ImageJ.

Statistical analysis

Statistical analyses were performed with GraphPad Prism 7.00, using unpaired two-tailed Student's *t*-tests, one-way or two-way ANOVA. All of the statistical tests performed are indicated in the figure legends. The data are presented as mean ± s.d. No statistical methods were used to predetermine sample size.

RNA-seq and computational analysis

MeSCs were purified from skin samples from control and stressed mice at telogen using FACS, based on their expression of CD117[7] and starting from a population that is negative for CD140A, CD45, SCA1 and CD34[57]. A total of 2 ng of RNA from each sample was used to generate RNA-seq libraries using a SMART-Seq v4 Ultra Low Input RNA kit (Takara, 634888) and Nextera XT DNA Library Preparation Kit (Illumina, FC-131-1024). Single-end sequencing reads were obtained using the Illumina NextSeq 500 platform. Sequencing reads from RNA-seq libraries were trimmed using Trim Galore! (https://www.bioinformatics.babraham.ac.uk/projects/trim_galore/) and aligned to the mouse reference genome (mm10) using STAR aligner[59]. Reads with alignment quality < Q30 were discarded. Gene expression levels were normalized and differential expression of genes was calculated using the DESeq2 package in R[60]. Gene set functional enrichment analysis was performed using DAVID[61,62]. Transcripts per million (TPM) calculated from count tables of control MeSC samples were used to determine the expression levels of adrenergic receptors and glucocorticoid receptor shown in Extended Data Fig. 3c.

Reporting summary

Further information on research design is available in the Nature Research Reporting Summary linked to this paper.

Data availability

The sequencing data that support the findings of this study have been deposited in the Gene Expression Omnibus (GEO) with the accession code GSE131566. Source data for all main figures and Extended Data figures are provided with the paper.

48. Hinoi, E. et al. The sympathetic tone mediates leptin's inhibition of insulin secretion by modulating osteocalcin bioactivity. *J. Cell Biol.* **183**, 1235–1242 (2008).

49. Abraira, V. E. et al. The cellular and synaptic architecture of the mechanosensory dorsal horn. *Cell* **168**, 295–310 (2017).
50. Pruitt, S. C., Freeland, A., Rusiniak, M. E., Kunnev, D. & Cady, G. K. Cdkn1b overexpression in adult mice alters the balance between genome and tissue ageing. *Nat. Commun*. **4**, 2626 (2013).
51. Szallasi, A. & Blumberg, P. M. Resiniferatoxin, a phorbol-related diterpene, acts as an ultrapotent analog of capsaicin, the irritant constituent in red pepper. *Neuroscience* **30**, 515–520 (1989).
52. Riol-Blanco, L. et al. Nociceptive sensory neurons drive interleukin-23-mediated psoriasiform skin inflammation. *Nature* **510**, 157–161 (2014).
53. Kashem, S. W. et al. Nociceptive sensory fibers drive interleukin-23 production from $CD301b^{+}$ dermal dendritic cells and drive protective cutaneous immunity. *Immunity* **43**, 515–526 (2015).
54. Marshall, I. C. B. et al. Activation of vanilloid receptor 1 by resiniferatoxin mobilizes calcium from inositol 1,4,5-trisphosphate-sensitive stores. *Br. J. Pharmacol*. **138**, 172–176 (2003).
55. Neubert, J. K. et al. Peripherally induced resiniferatoxin analgesia. *Pain* **104**, 219–228 (2003).
56. Watanabe, T., Sakurada, N. & Kobata, K. Capsaicin-, resiniferatoxin-, and olvanil-induced adrenaline secretions in rats via the vanilloid receptor. *Biosci. Biotechnol. Biochem*. **65**, 2443–2447 (2001).
57. Zhang, B., He, M. & Hsu, Y.-C. FACS isolation of melanocyte stem cells from mouse skin. *Protoc. Exch*. https://doi.org/10.21203/rs.2.17987/v1 (2019).
58. Gilchrest, B. A., Vrabel, M. A., Flynn, E. & Szabo, G. Selective cultivation of human melanocytes from newborn and adult epidermis. *J. Invest. Dermatol*. **83**, 370–376 (1984).
59. Dobin, A. et al. STAR: ultrafast universal RNA-seq aligner. *Bioinformatics* **29**, 15–21 (2013).
60. Love, M. I., Huber, W. & Anders, S. Moderated estimation of fold change and dispersion for RNA-seq data with DESeq2. *Genome Biol*. **15**, 550 (2014).
61. Huang, W., Sherman, B. T. & Lempicki, R. A. Bioinformatics enrichment tools: paths toward the comprehensive functional analysis of large gene lists. *Nucleic Acids Res*. **37**, 1–13 (2009).
62. Huang, W., Sherman, B. T. & Lempicki, R. A. Systematic and integrative analysis of large gene lists using DAVID bioinformatics resources. *Nat. Protocols* **4**, 44–57 (2009).

Acknowledgements We thank G. Karsenty for $Adrb2^{fl/fl}$ mice, D. Ginty for $TH^{creERT2}$ mice and many colleagues who donated mice to the Jackson Laboratory; A. Wagers, W. Anderson, C.-Y. Chang, Y. Fong, Q. Ma, M. Nahrendorf, A. Sahay and members of the Y.-C.H. laboratory, in particular M. Gonzalez-Celeiro, for discussions and comments on the manuscript; S. Kim, Y.-L. Kang and O. Chung for technical assistance; and HCBI, the HSCRB FACS core and histology core, FAS Small Molecule Mass Spectrometry Facility, Office of Animal Resources and the Bauer Core Facility at Harvard University for technical support. This work was supported in part by the Harvard Stem Cell Institute; Harvard NeuroDiscovery Center; Harvard Medical School Dean's Innovation Grant; Smith Family Foundation Odyssey Award; American Cancer Society (RSG-18-152-01-DDC); NIH (R01-AR070825 to Y.-C.H., R01 AR043369-23, R01CA222871, R01AR072304 and P01 CA163222 to D.E.F., R01CA103846 and P01CA163222 to L.I.Z. and DP2AT009499 and R01AI130019 to I.M.C.); and grants from the Dr. Miriam and Sheldon G. Adelson Medical Research Foundation to D.E.F. and from Klarman Cell Observatory to A.R. Y.-C.H. is a Pew Scholar and a NYSCF – Robertson Investigator; A.R. and L.I.Z. are HHMI investigators; B.Z. is a recipient of the Charles A. King Trust Postdoctoral Research Fellowship; M.H. is a recipient of the NSF Graduate Research Fellowships Program (DGE1745303) and was supported by the Joint Program in Molecules, Cells, and Organisms (5T32GM007598-40); Y. Shwartz is a Helen Hay Whitney postdoctoral fellow and a recipient of the Woman in Science Weizmann Institute of Science Award; T.M.C. had a CAPES/HARVARD fellowship for visiting professor from CAPES (Process no. 88881.162285/2017-01) and is supported by a FAPESP grant (2013/08216-2); E.M.F. was supported by a Leukemia & Lymphoma Society Scholar grant (5372-15); and J.D.B. and S.M. acknowledge support from the Broad Institute Fellows Program.

Author contributions B.Z. and Y.-C.H. conceived the project. B.Z. performed most of the experiments. S.M. performed bioinformatic analysis. I.R. and Y. Su performed the human melanocyte experiments. M.H. performed the immunostaining of sympathetic ganglia and quantifications of sympathetic nerve density. P.B. and I.M.C. made the initial observations of hair greying in RTX-injected mice. S.C. performed experiments related to chronic unpredictable stress and corticosterone feeding. Y. Shwartz performed the sympathetic nerve ablation experiments. W.A.G. and T.M.C. performed the guanethidine experiments. E.M.F. performed the radiation experiments. Y.-C.H., D.E.F., I.M.C., T.M.C., J.D.B., A.R. and L.I.Z. provided intellectual input and helped shape the research. B.Z. and Y-C.H. wrote the manuscript, with discussions and feedback from all co-authors.

Competing interests L.I.Z. is a founder and stockholder of Fate Therapeutics, Scholar Rock and CAMP4 Therapeutics. D.E.F. has a financial interest in Soltego, a company developing salt-inducible kinase inhibitors for topical skin-darkening treatments that might be used for a broad set of human applications. The interests of D.E.F. were reviewed and are managed by Massachusetts General Hospital and Partners HealthCare in accordance with their conflict of interest policies. A.R. is a member of the Scientific Advisory Board (SAB) of Thermo Fisher Scientific, Neogene Therapeutics, Asimov and Syros Pharmaceuticals; an equity holder of Immunitas; and a founder and an equity holder of Celsius Therapeutics. I.M.C. is an SAB member of GSK Pharmaceuticals and Kintai Therapeutics. A provisional patent application has been filed based on this work (applicants: President and Fellows of Harvard College and The General Hospital Corporation; inventors: Y.-C.H., B.Z., D.E.F. and I.R.; application number: 62/903,517; status: pending/provisional; aspect covered: methods and compositions for controlling hair greying). All of the other authors declare no competing interests.

Additional information

Supplementary information is available for this paper at https://doi.org/10.1038/s41586-020-1935-3.

Correspondence and requests for materials should be addressed to Y.-C.H.

Peer review information *Nature* thanks Salvador Aznar Benitah, Christopher Deppmann, William Lowry and the other, anonymous, reviewer(s) for their contribution to the peer review of this work.

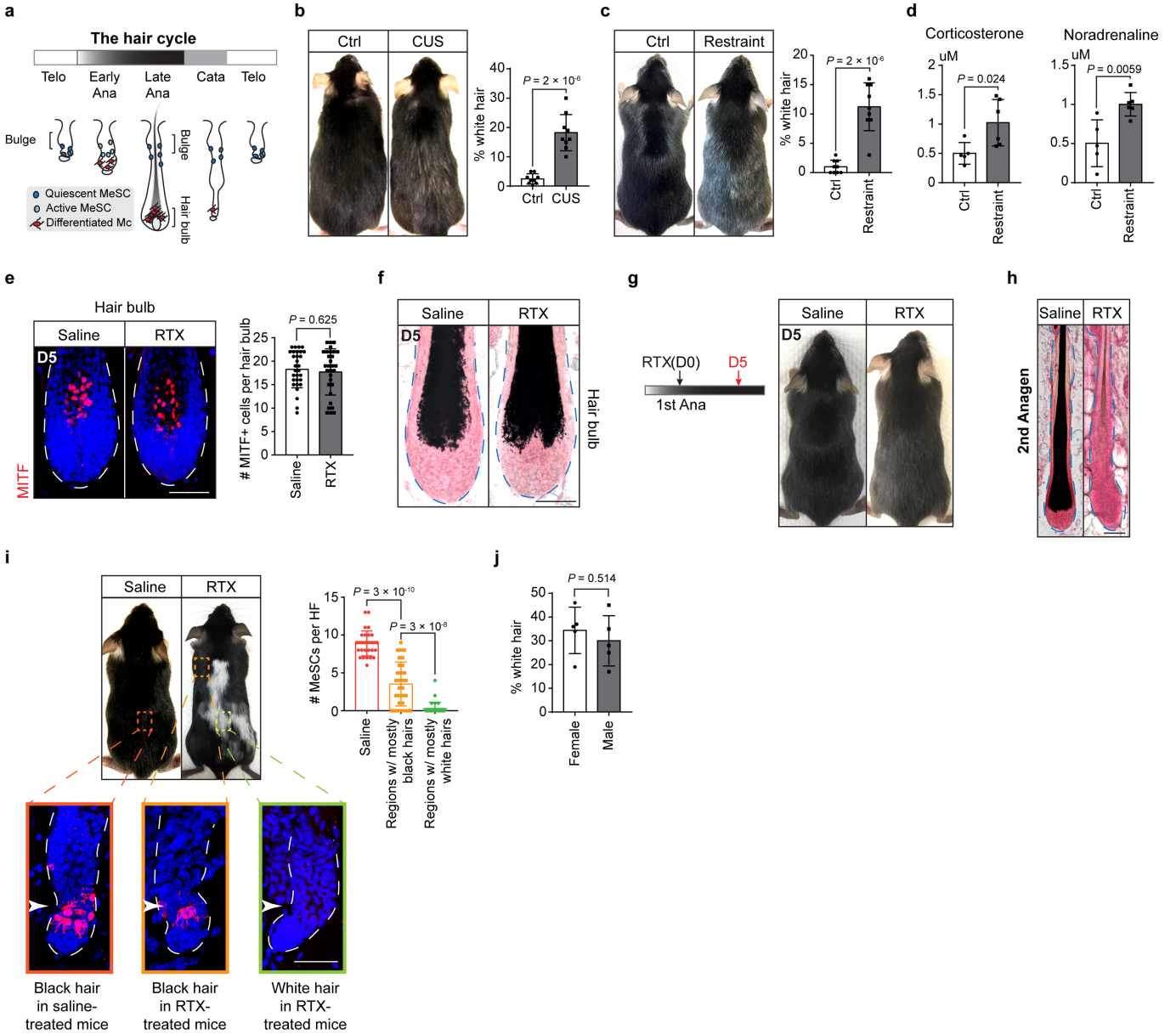

Extended Data Fig. 1 | Effects of stress on the hair pigmentation. a, Schematic of MeSC behaviour during the hair cycle. **b**, Hair greying after mice were subjected to chronic unpredictable stress. Quantifications were done by plucking around 100 hairs from different regions across the skin and counting the number of white hairs ($n = 9$ plucked regions from 3 mice for each condition, two-tailed unpaired t-test). **c**, Hair greying after mice were subjected to restraint stress. Quantifications as described in **b**. **d**, LC–MS/MS quantification of corticosterone and noradrenaline after restraint stress ($n = 5$ mice for control and $n = 6$ mice for restraint, two-tailed unpaired t-test). **e**, Left, immunofluorescent staining of hair bulbs for melanocyte-inducing transcription factor (MITF, red) from mice five days after treatment with saline or RTX. Right, quantification of MITF$^+$ cells ($n = 30$ hair follicles from 3 mice for each condition, two-tailed unpaired t-test). **f**, Fontana-Masson staining of hair bulbs for melanin from mice five days after treatment with saline or RTX ($n = 6$ mice for each condition). **g**, Coat colour in mice five days after RTX injection in anagen. RTX was injected in full anagen and the mice were examined five days later, at late anagen. The coat colour remained black ($n = 6$ mice for each condition). **h**, Fontana-Masson staining of hair follicles for melanin from mice that were treated with saline or RTX at first anagen and examined at second anagen (see Fig. 1e for corresponding fluorescent images) ($n = 6$ mice for each condition). **i**, Quantification of the number of MeSCs in the skin of mice injected with saline or RTX. For the RTX-injected mice, the numbers of MeSCs in regions with predominantly black hairs and regions with many white hairs are quantified separately. Orange and green dashed boxes denote representative black and white hair regions, respectively, in RTX-injected mice. Enlarged boxes show representative immunofluorescent images of hair follicles from each region. White arrowheads indicate regions where MeSCs reside ($n = 30$ hair follicles from 3 mice for each condition, one-way ANOVA with Tukey's multiple comparisons test). **j**, Quantification of the body area covered by white hairs in female versus male mice ($n = 5$ mice for each sex, two-tailed unpaired t-test). All data are mean ± s.d.

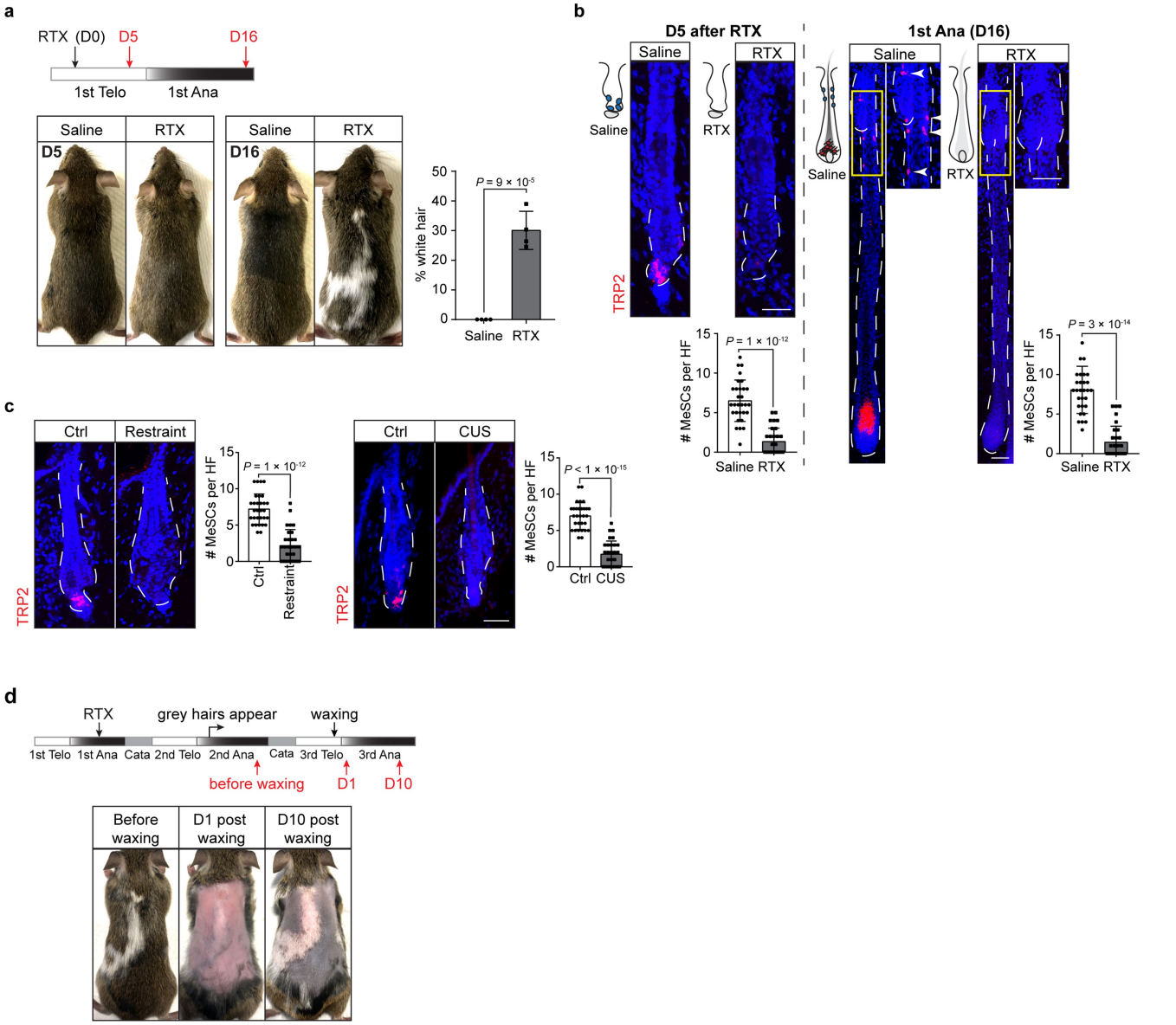

Extended Data Fig. 2 | Loss of MeSCs in three different models of stress. **a**, Top, schematic of experimental design for RTX injection in first telogen (red arrows indicate collection of skin samples). Bottom left, representative mouse images 5 days and 16 days after RTX injection in first telogen. Bottom right, quantification of the body area covered by white hairs 16 days after RTX injection ($n = 4$ mice for each condition, two-tailed unpaired t-test). **b**, Immunofluorescent staining for TRP2 from mice injected with saline or RTX in first telogen ($n = 30$ hair follicles from 4 mice for each condition, two-tailed unpaired t-test). Yellow boxes denote the upper region of the hair follicle, where MeSCs reside. Enlarged views of the yellow-boxed regions are shown to the right. White arrowheads indicate MeSCs. Quantifications of MeSCs are also shown (bottom). **c**, Immunofluorescent staining for TRP2 (red) (left) and quantification of MeSCs (right) from mice subjected to chronic unpredictable stress or restraint stress ($n = 30$ hair follicles from 5 mice for each condition, two-tailed unpaired t-test). **d**, Hair coat colour was monitored in RTX-injected mice for multiple rounds of hair-follicle regeneration (waxing was used to initiate new rounds of anagen) ($n = 3$ mice for each condition). Schematic denotes the experimental design. Scale bars, 50 μm. All data are mean ± s.d.

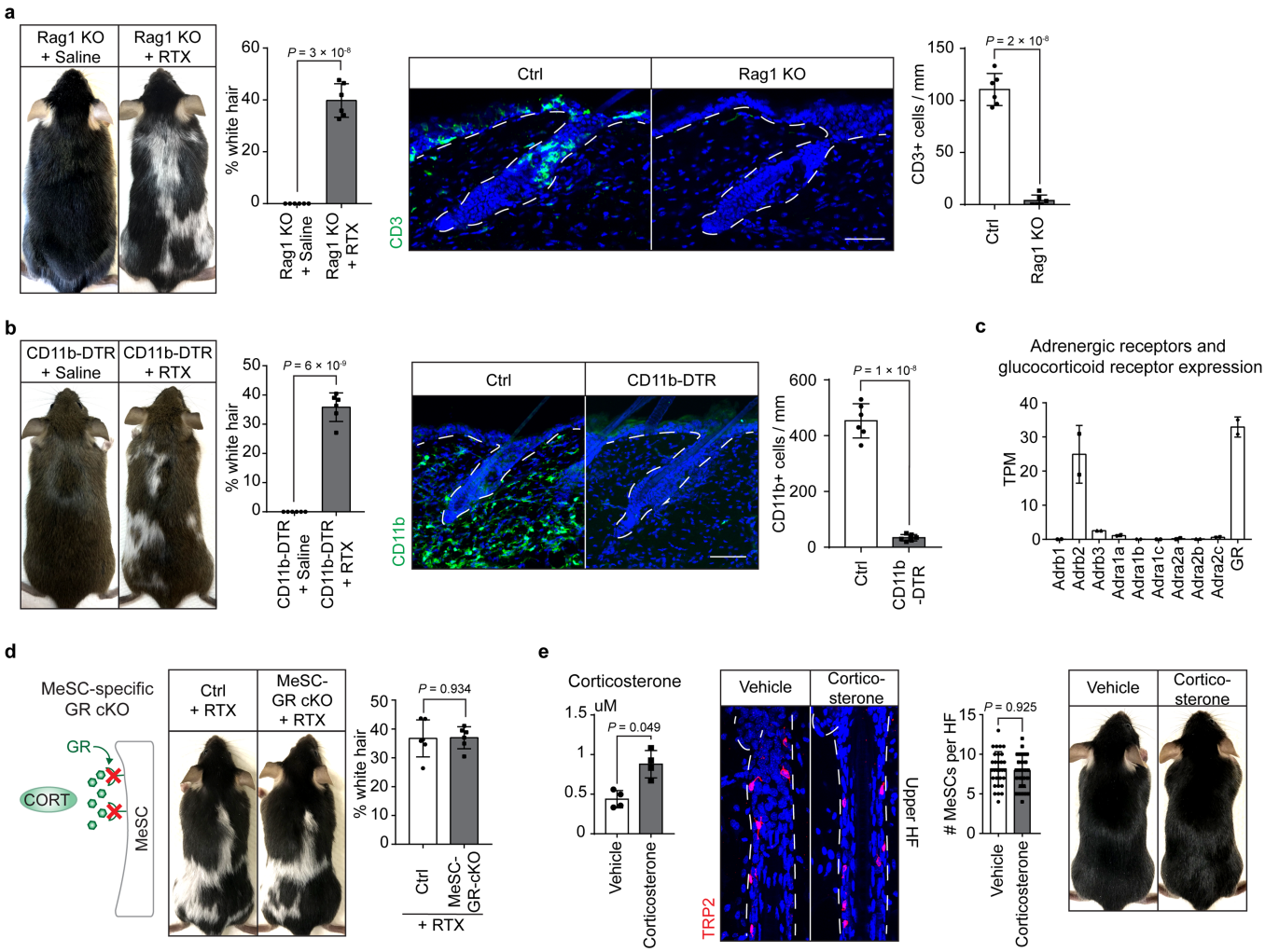

Extended Data Fig. 3 | Stress-induced hair greying is not mediated by corticosterone or immune attack. a, Left, formation of white hairs after RTX injection in *Rag1* mutant mice that are devoid of T and B cells (*Rag1* KO) ($n = 6$ for each condition, two-tailed unpaired *t*-test). Right, immunofluorescent staining for the T cell marker CD3 (green) in control and *Rag1* KO skin ($n = 6$ mice for each condition, two-tailed unpaired *t*-test). **b**, Left, hair greying occurs when RTX is injected into *CD11b-DTR* mice that were treated with diphtheria toxin to deplete myeloid cells ($n = 6$ mice for each condition). Right, immunofluorescent staining for CD11B (green) in skin from control and *CD11b-DTR* mice that were treated with diphtheria toxin ($n = 6$ mice for each condition). **c**, Expression of adrenergic receptors and glucocorticoid receptor (GR) in MeSCs ($n = 2$ biologically independent samples). **d**, Formation of white hairs after RTX injection into $Tyr^{creERT2}$;$GR^{fl/fl}$ mice (MeSC-*GR* cKO) ($n = 6$ mice for each condition, two-tailed unpaired *t*-test). **e**, Left, enzyme-linked immunosorbent assay (ELISA) measurement of the level of corticosterone in the blood three days after supplying corticosterone in the drinking water ($n = 4$ mice for each condition). Middle, immunofluorescent staining of hair follicles for TRP2 (red) from mice five days after treatment with corticosterone ($n = 30$ hair follicles from 3 mice for each condition, two-tailed unpaired *t*-test). Right, coat colour after hair follicles in corticosterone-treated mice enter another round of anagen to regenerate new hairs. Scale bars, 50 μm. All data are mean ± s.d.

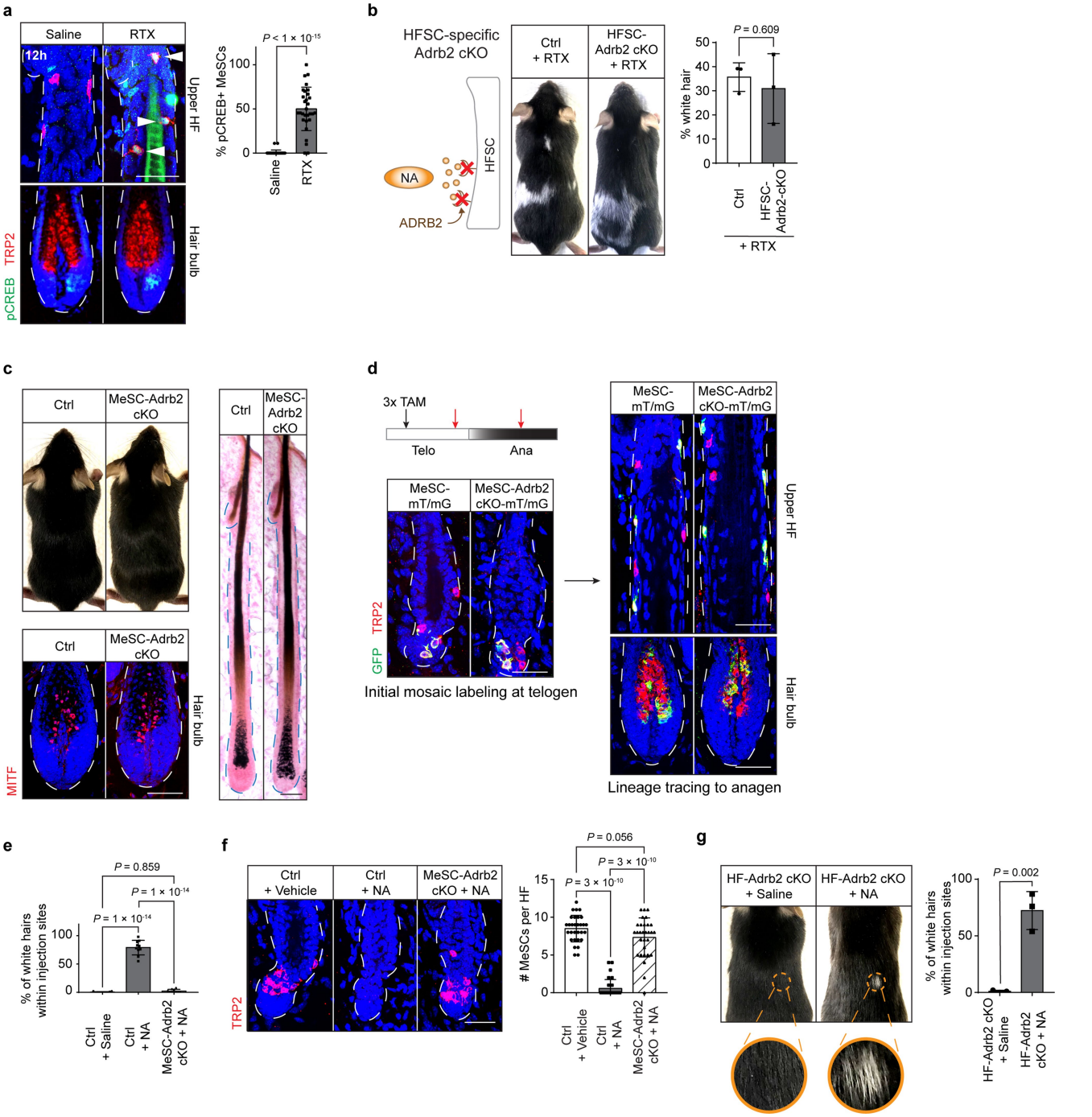

Extended Data Fig. 4 | Perturbations of the noradrenaline–ADRB2 pathway. **a**, Left, immunofluorescent staining of hair follicles for phosphorylated CREB (pCREB; green) and TRP2 (red) 12 h after RTX injection. Right, quantification of the percentage of pCREB$^+$ MeSCs ($n = 30$ hair follicles from 3 mice for each condition, two-tailed unpaired t-test). White arrowheads indicate pCREB$^+$ MeSCs in upper hair follicles after RTX injection. **b**, Formation of white hairs after RTX injection into *K15*^{crePGR};*Adrb2*$^{fl/fl}$ mice (HFSC-*Adrb2* cKO) ($n = 3$ mice for each condition, two-tailed unpaired t-test). **c**, Top left, coat colour in unstressed *Tyr*^{creERT2};*Adrb2*$^{fl/fl}$ mice (MeSC-*Adrb2* cKO) in the second telogen after treatment with tamoxifen (seven times) at the first telogen. Bottom left, immunofluorescent staining of hair bulbs for MITF (red) in *Tyr*^{creERT2};*Adrb2*$^{fl/fl}$ mice in anagen. Right, Fontana-Masson melanin staining of anagen hair follicles from *Tyr*^{creERT2};*Adrb2*$^{fl/fl}$ mice ($n = 3$ mice for each condition). **d**, Top left, schematic of experimental design for mosaic labelling in unstressed control and *Adrb2* knockout mice (red arrows indicate collection of skin samples). Bottom left, immunofluorescent staining for GFP (green) and TRP2 (red) from *Tyr*^{creERT2};*Rosa*$^{mT/mG}$ mice (MeSC-mT/mG) and *Tyr*^{creERT2};*Adrb2*$^{fl/fl}$;*Rosa*$^{mT/mG}$ mice (MeSC-*Adrb2* cKO-mT/mG) after treatment with tamoxifen (three times) at first telogen. Right, immunofluorescent staining of hair follicles for GFP (green) and TRP2 (red) after the mice enter anagen ($n = 3$ mice for each condition). **e**, Quantification of the percentage of white hairs after intradermal injection of saline or noradrenaline ($n = 10$ injected sites from 6–8 mice for each condition, one-way ANOVA with Tukey's multiple comparisons test). **f**, Left, immunofluorescent staining of hair follicles for TRP2 (red) from the skins of mice that were intradermally injected with noradrenaline ($n = 30$ hair follicles from 10 injection sites for each condition, one-way ANOVA with Tukey's multiple comparisons test). Right, quantification of MeSCs. **g**, White hairs are formed after intradermal injection of noradrenaline in *K15*^{crePGR};*Adrb2*$^{fl/fl}$ mice (HF-*Adrb2* cKO) ($n = 3$ injection sites for each condition, two-tailed unpaired t-test). Yellow dashed circles denote intradermal injection sites. Scale bars, 50 µm. All data are mean ± s.d.

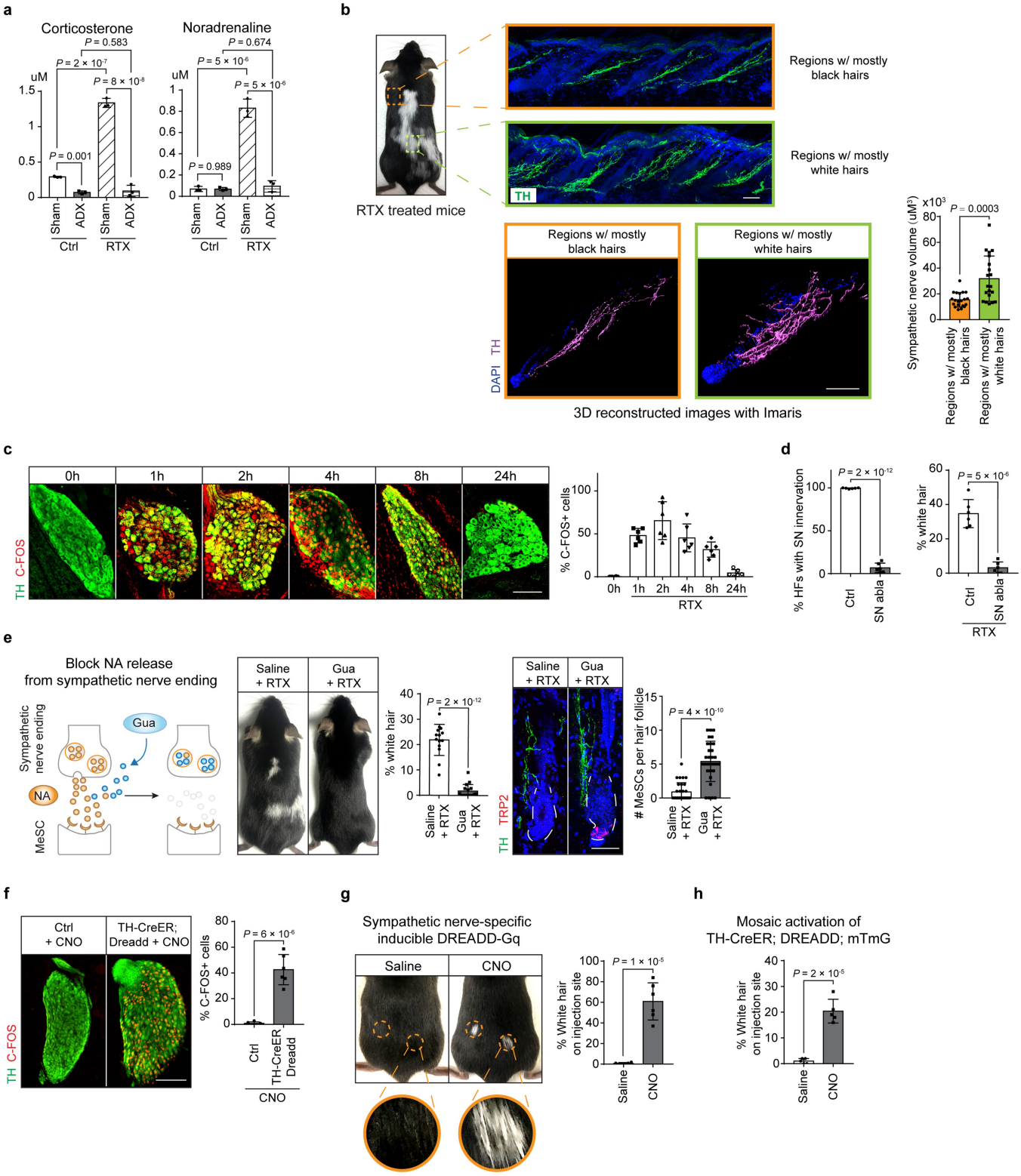

Extended Data Fig. 5 | See next page for caption.

Extended Data Fig. 5 | Activation of the sympathetic nervous system by nociception-induced stress or sympathetic-nerve-specific inducible G_q-DREADD. a, LC–MS/MS quantification of stress hormones in sham-operated and adrenalectomized mice ($n = 3$ mice for each condition, two-way ANOVA with Benjamini–Hochberg correction). **b**, Top, immunofluorescent staining of sympathetic nerves in the skin regions with predominantly black hairs (orange box) and with mostly white hairs (green box) ($n = 3$ mice for each condition). Bottom, 3D surfaces of tyrosine hydroxylase (TH) staining, created using Imaris software, and quantification of the sympathetic nerve volume from regions with different numbers of unpigmented hairs ($n = 20$ hair follicles for each region from 3 mice, two-tailed unpaired *t*-test). **c**, Left, immunofluorescent staining of sympathetic ganglia for tyrosine hydroxylase (green) and FOS (red) from mice injected with RTX. Cells were collected at different time points between 0 and 24 h. Right, quantification of FOS^+ cells ($n = 6$ sympathetic ganglia from 3 mice for each time point). **d**, Quantification of the efficiency of chemical sympathectomy ($n = 6$ mice for each condition, two-tailed unpaired *t*-test), and percentage of white hairs in RTX-injected mice treated with vehicle (ctrl) or 6-OHDA (SN abla) ($n = 6$ mice for each condition, two-tailed unpaired *t*-test). **e**, Guanethidine (gua) injection blocks the formation of white hairs that is induced by RTX injection (quantification for percentage of white hairs: $n = 14$ mice for each condition, two-tailed unpaired *t*-test; quantification for numbers of MeSCs: $n = 30$ hair follicles from 6 mice for each condition, two-tailed unpaired *t*-test). **f**, Left, immunofluorescent staining of sympathetic ganglia for tyrosine hydroxylase (green) and FOS (red) from $TH^{creERT2}$;*CAG-LSL-*G_q*-DREADD* mice that were injected with CNO; cells were collected 6 h later. Right, quantification of FOS^+ cells ($n = 6$ sympathetic ganglia from 2 mice for each condition, two-tailed unpaired *t*-test). **g**, Formation of white hairs after intradermal injection of CNO into $TH^{creERT2}$;*CAG-LSL-*G_q*-DREADD* mice ($n = 6$ injection sites from 5 mice for each condition, two-tailed unpaired *t*-test). Yellow dashed circles denote intradermal CNO injection sites. **h**, Quantification of the percentage of white hairs at CNO injection sites in mosaically induced $TH^{creERT2}$;*CAG-LSL-*G_q*-DREADD*;$Rosa^{mT/mG}$ mice ($n = 5$ injection sites from 4 mice for each condition, two-tailed unpaired *t*-test). Scale bars, 50 μm. All data are mean ± s.d.

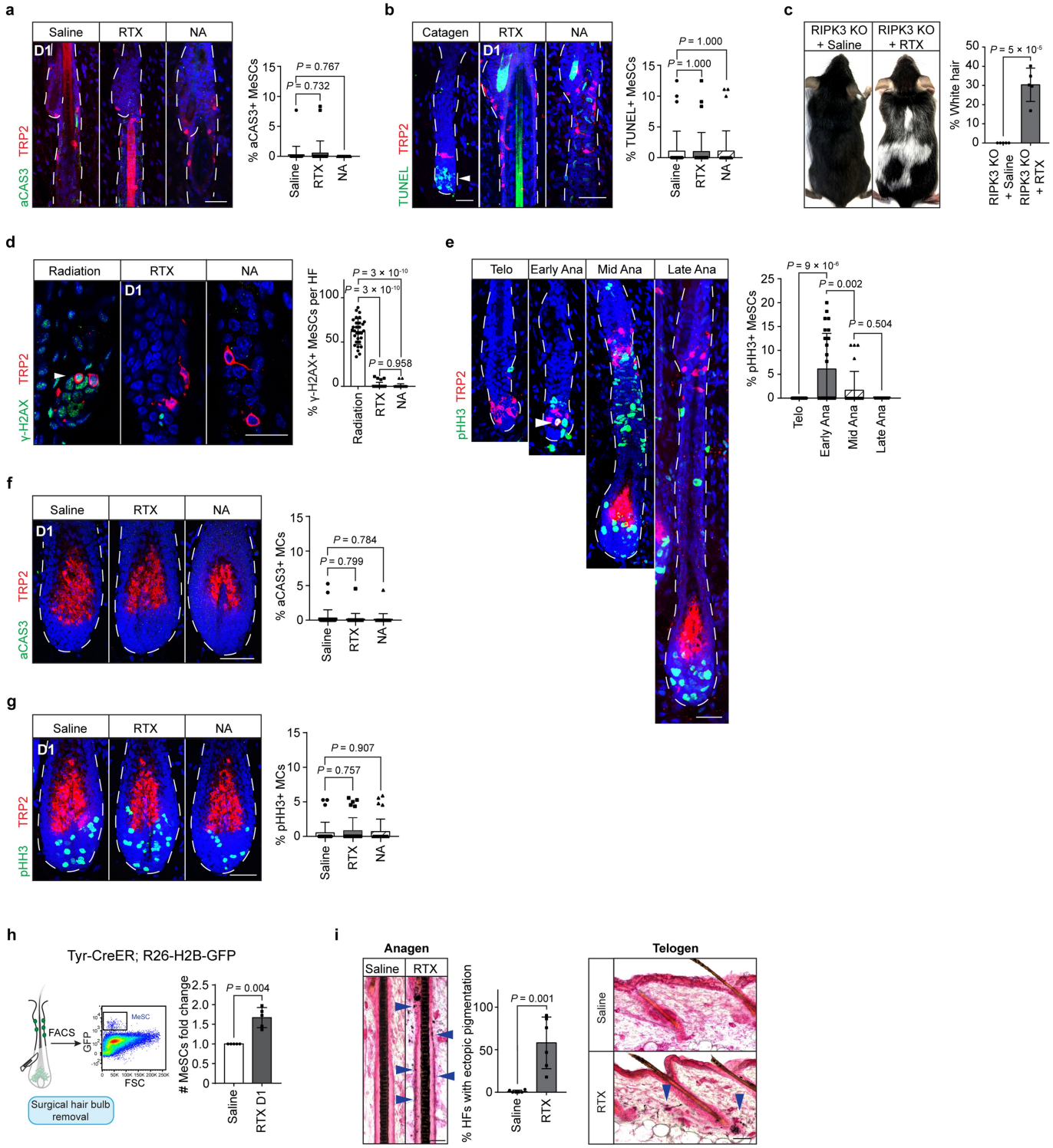

Extended Data Fig. 6 | See next page for caption.

Extended Data Fig. 6 | Analysis of apoptosis and proliferation of MeSCs and the effect of RTX or noradrenaline on mature melanocytes. a, Left, immunofluorescent staining of active caspase-3 (aCAS3; green) and TRP2 (red) from mice one day after injection with RTX or noradrenaline. Right, quantification of aCAS3$^+$ MeSCs (n = 30 hair follicles from 6 mice for each condition, one-way ANOVA with Tukey's multiple comparisons test). **b**, TUNEL assay of hair follicles from mice one day after treatment with RTX or noradrenaline. Catagen hair follicles were used as positive controls for TUNEL. White arrowhead points to apoptotic hair follicle cells (n = 30 hair follicles from 6 mice for each condition, one-way ANOVA with Tukey's multiple comparisons test). **c**, Formation of white hairs in *Ripk3* mutant mice (RIPK3 KO) injected with RTX (n = 5 mice for each condition, two-tailed unpaired t-test). **d**, Left, immunofluorescent staining of hair follicles for the DNA damage marker γ-H2AX (green) and TRP2 (red) from mice one day after treatment with RTX or noradrenaline. Hair follicles from irradiated mice were used as positive controls. White arrowhead indicates the MeSCs with DNA damage. Right, quantification of γ-H2AX$^+$ MeSCs (n = 30 hair follicles from 6 mice for each condition, one-way ANOVA with Tukey's multiple comparisons test). **e**, Left, immunofluorescent staining for phosphorylated histone H3 (pHH3; green) and TRP2 (red) of control hair follicles at different stages of the hair cycle. Right, quantification of pHH3$^+$ MeSCs (n = 25 hair follicles from 3 mice for each condition, one-way ANOVA with Tukey's multiple comparisons test). **f**, Left, immunofluorescent staining of hair bulbs for aCAS3 (green) and TRP2 (red) from mice one day after injection with RTX or noradrenaline. Right, quantification of aCAS3$^+$ mature melanocytes (MCs) (n = 30 hair follicles from 3 mice for each condition, one-way ANOVA with Tukey's multiple comparisons test). **g**, Left, immunofluorescent staining of hair bulbs for pHH3 (green) and TRP2 (red) from mice one day after injection with RTX or noradrenaline. Right, quantification of pHH3$^+$ mature melanocytes (n = 30 hair follicles from 3 mice for each condition, one-way ANOVA with Tukey's multiple comparisons test). **h**, Left, schematic of the strategy for isolation of MeSCs. Right, FACS analysis of the numbers of MeSCs one day after RTX injection (n = 5 mice for each condition, two-tailed unpaired t-test). **i**, Fontana-Masson melanin staining of anagen or telogen samples five days after injection of saline or RTX (n = 6 mice for each condition, two-tailed unpaired t-test). Blue arrowheads indicate ectopic pigments. Scale bars, 50 μm. All data are mean ± s.d.

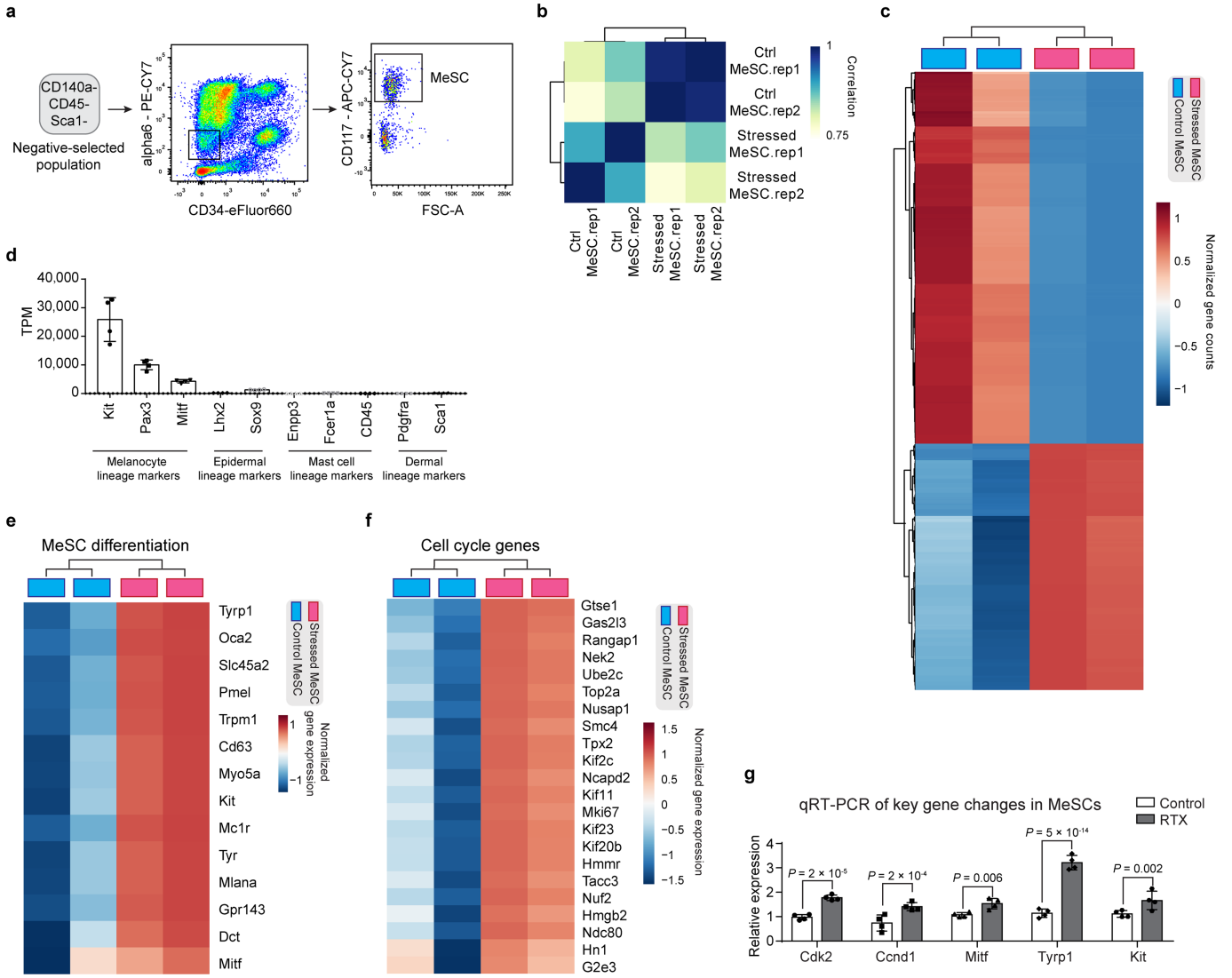

Extended Data Fig. 7 | Differential gene expression in normal and stressed MeSCs. a, FACS strategy for the purification of MeSCs. MeSCs were selected on the basis of their expression of CD117, from a population that is negative for CD140A, CD45, SCA1 and CD34 and that shows modest expression for integrin α6. **b**, Sample clustering based on Pearson's correlation of transcriptomes between control and stressed MeSCs ($n = 2$ biologically independent samples for each condition). **c**, Heat map of all differentially expressed genes ($n = 2$ biologically independent samples for each condition; *P* values were calculated using the Wald test implemented in DESeq2, and adjusted using the Benjamini–Hochberg method. Differentially expressed genes were those that had the absolute value of $\log_2$(gene expression in stressed versus control MeSCs) ≥ 0.58 and adjusted *P* value < 0.05. **d**, Expression levels of marker genes for different cell types in the skin, confirming the purity of MeSCs that were used for RNA-seq ($n = 4$ biologically independent samples). TPM, transcripts per million. **e**, Heat maps showing expression of signature genes that are related to the differentiation of MeSCs. **f**, Heat maps showing expression of cell-cycle signature genes. *Hn1* is also known as *Jpt1*. **g**, qRT–PCR validation of selected differentially expressed genes in FACS-purified mouse MeSCs from skins of control and RTX-injected mice ($n = 4$ biological replicates for each condition, two-way ANOVA with Benjamini–Hochberg correction). All data are mean ± s.d.

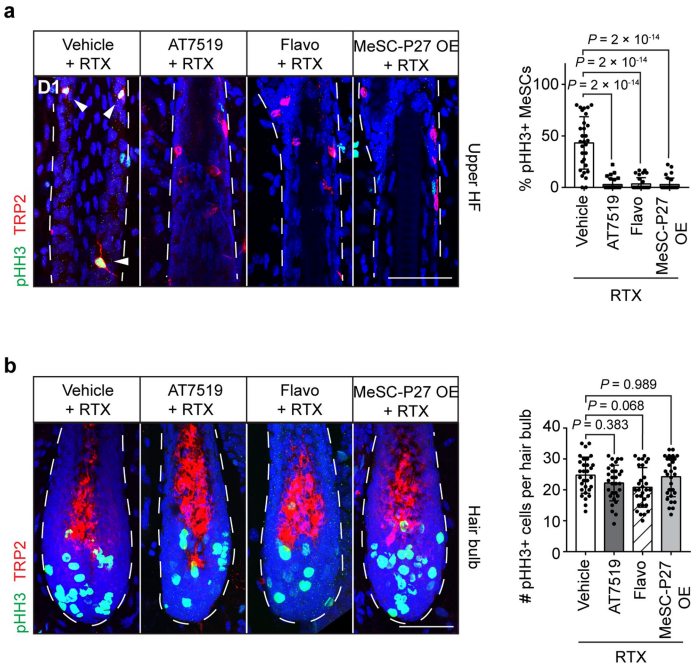

Extended Data Fig. 8 | Proliferation analysis of RTX-injected mice that were treated with CDK inhibitors chemically or genetically. a, **b**, Left, immunofluorescent staining of upper hair follicles (**a**) and hair bulbs (**b**) for pHH3 (green) and TRP2 (red) from mice one day after RTX injection, RTX injection with topical application of CDK inhibitors (AT7519 or flavopiridol) or RTX injection with MeSC-specific overexpression of P27 (MeSC-P27 OE). Right, quantification of pHH3$^+$ cells ($n = 30$ hair follicles from 3 mice for each condition, one-way ANOVA with Tukey's multiple comparisons test). Scale bars, 50 µm. All data are mean ± s.d.

nature research

Corresponding author(s): Ya-Chieh Hsu

Last updated by author(s): Dec 22, 2019

Reporting Summary

Nature Research wishes to improve the reproducibility of the work that we publish. This form provides structure for consistency and transparency in reporting. For further information on Nature Research policies, see Authors & Referees and the Editorial Policy Checklist.

Statistics

For all statistical analyses, confirm that the following items are present in the figure legend, table legend, main text, or Methods section.

n/a	Confirmed	
☐	☒	The exact sample size (*n*) for each experimental group/condition, given as a discrete number and unit of measurement
☐	☒	A statement on whether measurements were taken from distinct samples or whether the same sample was measured repeatedly
☐	☒	The statistical test(s) used AND whether they are one- or two-sided *Only common tests should be described solely by name; describe more complex techniques in the Methods section.*
☐	☒	A description of all covariates tested
☐	☒	A description of any assumptions or corrections, such as tests of normality and adjustment for multiple comparisons
☐	☒	A full description of the statistical parameters including central tendency (e.g. means) or other basic estimates (e.g. regression coefficient) AND variation (e.g. standard deviation) or associated estimates of uncertainty (e.g. confidence intervals)
☐	☒	For null hypothesis testing, the test statistic (e.g. *F*, *t*, *r*) with confidence intervals, effect sizes, degrees of freedom and *P* value noted *Give P values as exact values whenever suitable.*
☒	☐	For Bayesian analysis, information on the choice of priors and Markov chain Monte Carlo settings
☒	☐	For hierarchical and complex designs, identification of the appropriate level for tests and full reporting of outcomes
☒	☐	Estimates of effect sizes (e.g. Cohen's *d*, Pearson's *r*), indicating how they were calculated

Our web collection on statistics for biologists contains articles on many of the points above.

Software and code

Policy information about availability of computer code

Data collection	BD FACSDiva (8.0.2), ZEN 2.3 SP1 (black 64 bit)
Data analysis	ImageJ (1.52h), Imaris (x64 9.3.0), Prism (7.00), Trim Galore! (0.4.1), STAR (2.5.3), DESeq2 (1.22.2), FlowJo (v10.0.7), DAVID (6.8), RStudio (Version 1.1.453), R (3.5.1)

For manuscripts utilizing custom algorithms or software that are central to the research but not yet described in published literature, software must be made available to editors/reviewers. We strongly encourage code deposition in a community repository (e.g. GitHub). See the Nature Research guidelines for submitting code & software for further information.

Data

Policy information about availability of data

All manuscripts must include a data availability statement. This statement should provide the following information, where applicable:

- Accession codes, unique identifiers, or web links for publicly available datasets
- A list of figures that have associated raw data
- A description of any restrictions on data availability

Sequence data that support the findings of this study have been deposited in GEO with the accession codes GSE131566 (https://www.ncbi.nlm.nih.gov/geo/query/acc.cgi?acc=GSE131566).
Source data for all figures are provided with the paper.

Field-specific reporting

Please select the one below that is the best fit for your research. If you are not sure, read the appropriate sections before making your selection.

☒ Life sciences ☐ Behavioural & social sciences ☐ Ecological, evolutionary & environmental sciences

For a reference copy of the document with all sections, see nature.com/documents/nr-reporting-summary-flat.pdf

Life sciences study design

All studies must disclose on these points even when the disclosure is negative.

Sample size	Sample sizes were determined based on prior studies and literatures of the field using similar experimental paradigms.
Data exclusions	No data were excluded from analysis
Replication	For in vivo experiments using rodent, biological replicates and independent cohorts of mice were used; for in vitro experiments, biological replicates as well as technical triplicates were used to ensure reproducibility. All attempts at replication were successful.
Randomization	The mice were randomly assigned into different experimental groups whenever possible, except in experiments required specific genotypes.
Blinding	For LC-MS-MS analysis, RNA-seq library preparation, and sequencing, experimenters were blinded to experimental conditions. Blinding was not possible in mouse studies due to the need to identify specific genotypes or treat mice with different chemicals according to experimental designs.

Reporting for specific materials, systems and methods

We require information from authors about some types of materials, experimental systems and methods used in many studies. Here, indicate whether each material, system or method listed is relevant to your study. If you are not sure if a list item applies to your research, read the appropriate section before selecting a response.

Materials & experimental systems

n/a	Involved in the study
☐	☒ Antibodies
☒	☐ Eukaryotic cell lines
☒	☐ Palaeontology
☐	☒ Animals and other organisms
☒	☐ Human research participants
☒	☐ Clinical data

Methods

n/a	Involved in the study
☒	☐ ChIP-seq
☐	☒ Flow cytometry
☒	☐ MRI-based neuroimaging

Antibodies

Antibodies used

TRP2 (Santa Cruz, CAT 10451, Clone D18, Lot k2114, Dilution 1:400)
Tyrosine hydroxylase (Millipore, CAT AB152, Clone N/A, Lot 3072361, Dilution 1:1000)
Tyrosine hydroxylase (Millipore, CAT AB1542, Clone N/A, Lot 3168710, Dilution 1:150-1:300)
c-Fos (Abcam, CAT 190289, Clone N/A, Lot GR3253255-1, Dilution 1:400)
γ-H2AX (Cell Signaling Technology, CAT 9718, Clone 20E3, Lot 17, Dilution 1:400)
Phospho-Histone H3 (Cell Signaling Technology, CAT 3377S, Clone D2C8, Lot 7, Dilution 1:250)
Cleaved Caspase-3 (Cell Signaling Technology, CAT 9664S, Clone 5A1E, Lot 45, Dilution 1:300)
GFP (Abcam, CAT ab290, Clone N/A, Lot N/A, Dilution 1:800)
CD3 (eBioscience, CAT 14-0032-81, Clone 17A2, Lot 4342633, Dilution 1:800)
CD11b (eBioscience, CAT 14-0112-81, Clone M1/70, Lot E03529-1632, Dilution 1:400)
Phospho-CREB (Cell Signaling Technology, CAT 9198, Clone 87G3, Lot 14, Dilution 1:800)
MITF (Abcam, CAT ab12039, Clone C5, Lot GR3206967-1, Dilution 1:400)
CD140a (Invitrogen, CAT 13-1401-82, Clone APA5, Lot 1993111, Dilution 1:200)
CD45 (Invitrogen, CAT 13-0451-82, Clone 30-F11, Lot 1989134, Dilution 1:400)
Sca1 (Invitrogen, CAT 13-5981-82, Clone D7, Lot 4346548, Dilution 1:1000)
CD34 (Invitrogen, CAT 13-0341-82, Clone RAM34, Lot 1993111, Dilution 1:100)
CD117 (Biolegend, CAT 135136, Clone ACK2, Lot B251908, Dilution 1:400)

Validation

TRP2 (Santa Cruz, CAT 10451): Mouse, Immunohistochemistry, validated on manufactures's website: http://www.emdmillipore.com/US/en/product/Anti-Tyrosine-Hydroxylase-Antibody,MM_NF-AB152#overview

Tyrosine hydroxylase (Millipore, CAT AB152): Mouse, Immunohistochemistry, validated on manufactures's website: http://

www.emdmillipore.com/US/en/product/Anti-Tyrosine-Hydroxylase-Antibody,MM_NF-AB152#overview

Tyrosine hydroxylase (Millipore, CAT AB1542): Mouse, Immunohistochemistry, validated on manufactures's website:http://www.emdmillipore.com/US/en/product/Anti-Tyrosine-Hydroxylase-Antibody,MM_NF-AB1542#overview

c-Fos (Abcam, CAT 190289, Clone N/A): Mouse, Immunohistochemistry, validated on manufactures's website: https://www.abcam.com/c-fos-antibody-ab190289.html#top-500

γ-H2AX (Cell Signaling Technology, CAT 9718): Mouse, Immunohistochemistry, validated on manufactures's website: https://www.cellsignal.com/products/primary-antibodies/phospho-histone-h2a-x-ser139-20e3-rabbit-mab/9718

Phospho-Histone H3 (Cell Signaling Technology, CAT 3377S): Mouse, Immunohistochemistry, validated on manufactures's website: https://www.cellsignal.com/products/primary-antibodies/phospho-histone-h3-ser10-d2c8-xp-rabbit-mab/3377

Cleaved Caspase-3 (Cell Signaling Technology, CAT 9664S): Mouse, Immunohistochemistry, validated on manufactures's website: https://www.cellsignal.com/products/primary-antibodies/cleaved-caspase-3-asp175-5a1e-rabbit-mab/9664

GFP (Abcam, CAT ab290, Clone N/A): Mouse, Immunohistochemistry, validated on manufactures's website: https://www.abcam.com/gfp-antibody-chip-grade-ab290.html?productWallTab=ShowAll

CD3 (eBioscience, CAT 14-0032-81, Clone 17A2): Mouse, Immunohistochemistry, validated on manufactures's website: https://www.thermofisher.com/antibody/product/CD3-Antibody-clone-17A2-Monoclonal/14-0032-82

CD11b (eBioscience, CAT 14-0112-81, Clone M1/70): Mouse, Immunohistochemistry, validated on manufactures's website: https://www.thermofisher.com/antibody/product/CD11b-Antibody-clone-M1-70-Monoclonal/14-0112-82

Phospho-CREB (Cell Signaling Technology, CAT 9198): Mouse, Immunohistochemistry, validated on manufactures's website: https://www.cellsignal.com/products/primary-antibodies/phospho-creb-ser133-87g3-rabbit-mab/9198

MITF (Abcam, CAT ab12039, Clone C5): Mouse, Immunohistochemistry, validated on manufactures's website: https://www.abcam.com/mitf-antibody-c5-chip-grade-ab12039.html

CD140a (Invitrogen, CAT 13-1401-82, Clone APA5): Mouse, FACS, validated on manufactures's website: https://www.thermofisher.com/antibody/product/CD140a-PDGFRA-Antibody-clone-APA5-Monoclonal/13-1401-82

CD45 (Invitrogen, CAT 13-0451-82, Clone 30-F11): Mouse, FACS, validated on manufactures's website: https://www.thermofisher.com/antibody/product/CD45-Antibody-clone-30-F11-Monoclonal/13-0451-82

Sca1 (Invitrogen, CAT 13-5981-82, Clone D7): Mouse, FACS, validated on manufactures's website: https://www.thermofisher.com/antibody/product/Ly-6A-E-Sca-1-Antibody-clone-D7-Monoclonal/13-5981-82

CD34 (Invitrogen, CAT 13-0341-82, Clone RAM34): Mouse, FACS, validated on manufactures's website: https://www.thermofisher.com/antibody/product/CD34-Antibody-clone-RAM34-Monoclonal/13-0341-82

CD117 (Biolegend, CAT 135136, Clone ACK2): Mouse, FACS, validated on manufactures's website: https://www.biolegend.com/en-us/products/apccyanine7-anti-mouse-cd117-c-kit-antibody-13795

Animals and other organisms

Policy information about studies involving animals; ARRIVE guidelines recommended for reporting animal research

Laboratory animals	C57BL/6J, Tyr-CreER, K15-CrePGR, Rag1 KO, CD11b-DTR, GR flox, Dreadd flox, Rosa-H2BGFP/mCherry, Rosa26-rtTA, Rosa-mTmG, RIPK3 knockout, Adrb2 flox, TH-CreER, pTRE-P27. All experiments used balanced groups of male and female mice. All experiments are conducted and compared using mice of the same hair cycle stage in comparable age range (P20-P25 for 1st telogen, P31-P36 for full anagen, and P50-P60 for 2nd telogen, or long-term monitoring as specified).
Wild animals	This study did not involve wild animals.
Field-collected samples	This study did not involve field-collected samples.
Ethics oversight	All animals were maintained in an Association for Assessment and Accreditation of Laboratory Animal Care-approved animal facility at Harvard University, Harvard Medical School, and Ribeirao Preto Medical School. Procedures were approved by the Institutional Animal Care and Use Committee of all institutions and were in compliance with all relevant ethical regulations.

Note that full information on the approval of the study protocol must also be provided in the manuscript.

Flow Cytometry

Plots

Confirm that:

☒ The axis labels state the marker and fluorochrome used (e.g. CD4-FITC).

☒ The axis scales are clearly visible. Include numbers along axes only for bottom left plot of group (a 'group' is an analysis of identical markers).

☒ All plots are contour plots with outliers or pseudocolor plots.

☒ A numerical value for number of cells or percentage (with statistics) is provided.

Methodology

Sample preparation	Mouse dorsal skin was collected, and the fat layer was removed by gentle scrapping from the dermal side. The skin was incubated in 0.25% collagenase in HBSS at 37 °C for 35-45 minutes on an orbital shaker. Single cell suspension was collected by gentle scraping of the dermal side and filtering through 70 µm and 40 µm filters. The epidermal layer was incubated in trypsin-EDTA at 37 °C for 35-45 minutes on an orbital shaker. Single cell suspension was collected by gentle scraping of the epidermal side and filtering through 70 µm and 40 µm filters. The single cell suspension was centrifuged for 5 minutes at 4°C, resuspended in 0.25% FBS in PBS, and stained with fluorescent dye-conjugated antibodies for 30 minutes. For late anagen skin samples, the bottom parts of the hair follicles containing mature melanocytes were removed by gentle scrapping under dissection microscope. The MeSCs located close to the bulge remained and were verified by immunostaining.
Instrument	FACS: BD FACSAria III
Software	BD FACSDiva (8.0.2), FlowJo (v10.0.7)
Cell population abundance	For sorting for RNA-seq, at least 10,000 MeSCs were collected. The purity was verified by expression of GFP driven by lineage specific CreER.
Gating strategy	Positive and negative gates were set using fluorescence minus one (FMO) background intensity controls. Fluorophores were chosen to minimize spectral overlap.

☒ Tick this box to confirm that a figure exemplifying the gating strategy is provided in the Supplementary Information.